The Plant Cell, Vol. 31: 1539–1562, July 2019, www.plantcell.org © 2019 ASPB.

The Ca^{2+} Channel CNGC19 Regulates Arabidopsis Defense Against Spodoptera Herbivory

Mukesh Kumar Meena,[a] Ramgopal Prajapati,[a,1] Deepthi Krishna,[a,1] Keerthi Divakaran,[b] Yogesh Pandey,[b] Michael Reichelt,[c] M.K. Mathew,[b] Wilhelm Boland,[c] Axel Mithöfer,[c] and Jyothilakshmi Vadassery[a,2]

[a] National Institute of Plant Genome Research, Aruna Asaf Ali Marg, New Delhi 110067, India
[b] National Centre for Biological Sciences, Tata Institute of Fundamental Research, Bangalore, Karnataka 560065, India
[c] Max Planck Institute for Chemical Ecology, Hans-Knöll-Straße 8, 07745 Jena, Germany

ORCID IDs: 0000-0002-8847-2023 (M.M.); 0000-0001-5969-3989 (R.P.); 0000-0002-5120-245X (D.K.); 0000-0001-7927-7034 (K.D.); 0000-0001-5721-1835 (Y.P.); 0000-0002-6691-6500 (M.R.); 0000-0002-5932-3598 (M.K.M.); 0000-0001-6784-2534 (W.B.); 0000-0001-5229-6913 (A.M.); 0000-0001-6296-7135 (J.V.)

Cellular calcium elevation is an important signal used by plants for recognition and signaling of environmental stress. Perception of the generalist insect, *Spodoptera litura*, by Arabidopsis (*Arabidopsis thaliana*) activates cytosolic Ca^{2+} elevation, which triggers downstream defense. However, not all the Ca^{2+} channels generating the signal have been identified, nor are their modes of action known. We report on a rapidly activated, leaf vasculature- and plasma membrane-localized, CYCLIC NUCLEOTIDE GATED CHANNEL19 (CNGC19), which activates herbivory-induced Ca^{2+} flux and plant defense. Loss of *CNGC19* function results in decreased herbivory defense. The *cngc19* mutant shows aberrant and attenuated intravascular Ca^{2+} fluxes. CNGC19 is a Ca^{2+}-permeable channel, as hyperpolarization of CNGC19-expressing *Xenopus* oocytes in the presence of both cyclic adenosine monophosphate and Ca^{2+} results in Ca^{2+} influx. Breakdown of Ca^{2+}-based defense in *cngc19* mutants leads to a decrease in herbivory-induced jasmonoyl-l-isoleucine biosynthesis and expression of JA responsive genes. The *cngc19* mutants are deficient in aliphatic glucosinolate accumulation and hyperaccumulate its precursor, methionine. CNGC19 modulates aliphatic glucosinolate biosynthesis in tandem with BRANCHED-CHAIN AMINO ACID TRANSAMINASE4, which is involved in the chain elongation pathway of Met-derived glucosinolates. Furthermore, CNGC19 interacts with herbivory-induced CALMODULIN2 in planta. Together, our work reveals a key mechanistic role for the Ca^{2+} channel CNGC19 in the recognition of herbivory and the activation of defense signaling.

INTRODUCTION

The common cutworm, *Spodoptera litura* (Lepidoptera: Noctuidae), is a widespread and destructive agriculture pest, causing defoliation and crop loss in economically important crops throughout Asia, Australia, and the Pacific Islands (Fand et al., 2015). Plants combat insect herbivory by constitutive defenses like structural barriers, and induced defenses like the production of phytohormones, secondary metabolites, and volatile organic compounds (Mithöfer and Boland, 2012). Genome sequencing of *S. litura* has identified massively expanded gene families that encode receptors for toxic compounds and detoxification enzymes, counteracting the induced defense arsenal and posing a great threat to agriculture (Cheng et al., 2017). Plant defense against herbivores is mediated by a jasmonic acid (JA)-dependent signaling cascade. Activation of the jasmonate pathway in Arabidopsis (*Arabidopsis thaliana*) triggers the production of antinutritive proteins, such as trypsin inhibitors and laccase-like multicopper oxidase, and secondary metabolites, such as glucosinolates (GSs; Van Poecke, 2007; Lan et al., 2014). The process by which insect herbivore attack is rapidly detected, as well as the signal transduction pathway that triggers defense mechanisms, are poorly understood. Plants sense herbivore insects by wound recognition, self-damage cues (damage-associated molecular patterns [DAMPs]), and insect elicitor cues (herbivore-associated molecular patterns [HAMPs]). Recognition of HAMPs/DAMPs by their cognate receptors triggers ion fluxes (Ca^{2+}) at the plasma membrane, a rapid production of reactive oxygen species and nitric oxide, phosphorylation events, and hormonal perturbations, forming a signaling network that coordinately controls local and systemic defense (Seybold et al., 2014; Zebelo and Maffei, 2015).

Plants respond to Spodoptera herbivory and wounding with rapid activation of electrical signals and elevation of cytosolic calcium (Ca^{2+}) in the wounded leaf (Maffei et al., 2004; Vadassery et al., 2012; Mousavi et al., 2013). Arabidopsis transmits this information through a long-distance signaling system to rapidly activate defense responses in unwounded systemic leaves connected by vasculature (Mousavi et al., 2013; Kiep et al., 2015). Systemic electrical signaling mediated by glutamate receptor (GLR)-type cation channels leads to activation of jasmonate biosynthesis in distal leaves (Mousavi et al., 2013). The *glr3.3 glr3.6* double mutant attenuates both wound-activated electrical and Ca^{2+} signal propagation between leaves (Mousavi et al., 2013; Nguyen et al., 2018; Toyota et al., 2018). GLR3.3 and GLR3.6 and TWO-PORE CHANNEL1 (TPC1) ion channels have been implicated in the elevation of local Ca^{2+} on feeding by aphids (Vincent et al., 2017). Recent work has identified that the amino

[1] These authors contributed equally to this work.
[2] Address correspondence to: jyothi.v@nipgr.ac.in.
The author responsible for distribution of materials integral to the findings presented in this article in accordance with the policy described in the Instructions for Authors (www.plantcell.org) is: Jyothilakshmi Vadassery (jyothi.v@nipgr.ac.in).
www.plantcell.org/cgi/doi/10.1105/tpc.19.00057

IN A NUTSHELL

Background: Insect herbivory greatly limits plant growth and productivity. The common cutworm *Spodoptera litura* is a widespread, destructive pest of diverse plants. Plants must rapidly respond to insect herbivory, which feed quickly. Cellular calcium (Ca^{2+}) elevation is an important signal used by plants for recognizing and responding to environmental stress. Plants respond to Spodoptera herbivory and wounding by elevating cytosolic Ca^{2+} in the wounded leaf. Elevation of Ca^{2+} requires Ca^{2+} entry either across the plasma membrane or from intracellular compartments via Ca^{2+} channels. The early steps of herbivory perception, the Ca^{2+} channels involved, and the signal transduction pathway that triggers plant defense mechanisms are poorly understood.

Question: The intense pain produced by a bite from the coral snake is due to activation of several acid-sensing ion channels in higher organisms, including humans. In a similar vein, does a plant sense an insect bite using Ca^{2+} ion channels and how does it activate plant defense?

Findings: Using the model plant *Arabidopsis thaliana* and the insect herbivore *Spodoptera litura*, we identified the Ca^{2+} channels involved in herbivory recognition. We demonstrated that a novel cyclic nucleotide-gated, Ca^{2+} channel, CNGC19, perceives herbivory and activates plant defense. *CNGC19* is expressed in leaf vasculature and is crucial for wound-induced intra-vascular Ca^{2+} fluxes. Loss of *CNGC19* function results in decreased herbivory defense, and aberrant wound-induced Ca^{2+} fluxes. Breakdown of Ca^{2+}-based defence in *cngc19* loss-of-function mutants leads to decreased herbivory-induced jasmonate biosynthesis. *cngc19* mutants are deficient in aliphatic glucosinolate accumulation and hyperaccumulate its precursor, methionine. Glucosinolates are crucial secondary metabolites in insect deterrence. CNGC19 modulates aliphatic glucosinolate biosynthesis in tandem with *BCAT4*, which functions in the chain elongation pathway of Met-derived glucosinolates. Thus, the Ca^{2+} channel CNGC19 has a key mechanistic role in recognizing herbivory and activating defense signaling.

Next steps: Identifying protein complexes of CNGC19 with other CNGCs and other putative subunits expressed in the vasculature would be an exciting area of research. Future biochemical studies on single and multiple CNGC mutants will be necessary to elucidate the role of this channel in generating both local and systemic Ca^{2+} elevation upon *S. litura* herbivory.

acid glutamate acts as a DAMP, and activates GLR ion channels when the specialist herbivore *Pieris rapae* feeds on Arabidopsis (Toyota et al., 2018). From all these reports it is clear that Ca^{2+} elevation upon herbivory is a complex process and involves multiple channels and pathways regulating local and long-distance Ca^{2+} signals.

Elevation of Ca^{2+}_{cyt} upon stress perception requires Ca^{2+} entry either across the plasma membrane or from intracellular compartments. In Arabidopsis, ligand-gated channels like cyclic nucleotide-gated channels (CNGCs), GLRs, stretch-activated Ca^{2+} channel OSCAs (reduced hyperosmolality-induced Ca^{2+} increases), and MID1-complementing activity (MCA) families are the four main plasma membrane Ca^{2+}-permeable channels, whereas the TPC1 is the key vacuolar channel (Dodd et al., 2010). CNGCs are a superfamily of cation channels that are permeable to divalent and monovalent cations, including Ca^{2+} and K^+. They are tetrameric proteins, each subunit having a cytosolic N- terminus, six transmembrane helices (S1 to S6) with a pore-forming region spanning S5 to S6, and a C-terminal cytosolic tail with binding domains for cyclic nucleotides (CNBD), and calmodulin (CaM) binding domains. Binding of cAMP and/or cGMP to the CNBD results in opening of the channel. Ca^{2+} binds to CaM on elevation of cytosolic Ca^{2+} (Ca^{2+}_{cyt}), and Ca^{2+}/CaM binds to the CaM binding domains. The traditional model posits that binding of Ca^{2+}/CaM prevents the binding of cNMPs to the channel, thereby closing the channel (Kaplan et al., 2007; Swarbreck et al., 2013). However, the current view is that CaM can both positively and negatively regulate CNGC as shown in CNGC12 (DeFalco et al., 2016). The Arabidopsis genome encodes 20 members of the CNGC family known to be involved in the response to abiotic, biotic, and developmental cues (Meena and Vadassery, 2015). Four CNGC channels (CNGC2, CNGC4, CNGC11, and CNGC12) have been well-studied for their role in DAMP-triggered and R-gene–mediated immune responses. CNGC2 and the corresponding null mutants *dnd1* (*defense*, *no death1* and *cngc4*/*dnd2* exhibit a lesion-mimic phenotype, constitutive *PR* gene expression, high salicylic acid (SA) levels, and lack of hypersensitive response upon pathogen inoculation (Clough et al., 2000; Balagué et al., 2003; Jurkowski et al., 2004). CNGC2-dependent elevation of Ca^{2+}_{cyt} upon perception of peptide DAMP, *At*Peps by the Pep receptor (PEPR) is known to mediate immune signal transduction (Qi et al., 2010; Ma et al., 2012). Moreover, CNGC2 is involved in jasmonate-induced Ca^{2+} mobilization (Lu et al., 2016). Chimeric *CNGC11* and *CNGC12* are responsible for the gain-of-function mutant constitutively expressing PR-genes (*cpr22*). The mutant displays autoimmune phenotypes with increased SA accumulation (Yoshioka et al., 2001; Urquhart et al., 2007). Recently a gain-of-function mutation (*brush*) in *Lotus japonicus* CNGC.IVA1 has been identified that co-assembles with wild-type subunits to form leaky channels and impairs infection by nitrogen-fixing rhizobia. Phylogenetic and synteny analysis revealed that *brush* (CNGC.IVA1) is orthologous to AtCNGC19 and AtCNGC20 (Chiasson et al., 2017).

We hypothesized that because there are rapid, spatially and temporally regulated Ca^{2+} elevations in local and systemic leaves upon Spodoptera herbivory, a suite of ion channels must be involved in generating these Ca^{2+} fluxes and activating specific downstream defenses. In this study, we elucidate the role of the Ca^{2+}-permeable channel, CNGC19, in the perception of herbivory and downstream defense. No reports on the involvement of any

CNGCs in plant-herbivore defense are currently available. We establish a key functional role for the ion channel CNGC19 in Arabidopsis defense against *S. litura*, via Ca^{2+}-mediated defense signaling that modulates phytohormones and secondary metabolites. Our study also points to the concerted action of different Ca^{2+} channels in the highly specific plant response to wounding and herbivory apart from the well-studied GLRs.

RESULTS

CNGC19 Is Activated in Local and Systemic Leaves upon Wounding and *S. litura* Herbivory

To identify the expression of early signaling genes involved in the interaction between Arabidopsis and Spodoptera, gene expression of mechanically wounded leaves (W) with or without *S. litura* oral secretion (OS) treatment (W+OS, W+Water) for 30 min each was compared using an Affymetrix array (J. Vadassery and A. Mithöfer, unpublished data). Insect OS application to artificial wounds can mimic herbivory (Maffei et al., 2004; Vadassery et al., 2012). Microarray data revealed that the gene encoding the cyclic nucleotide-gated channel, *CNGC19* (At3g17690), was highly upregulated. Using quantitative real-time PCR we confirmed the data and found that both wounding and application of *S. litura* OS elevated *CNGC19* transcript levels, in as little as 15 min and peaked at 1 h. *S. litura* OS amplified the *CNGC19* expression over simple wounding (30-fold and 12-fold, respectively, above control; Figure 1A). Expression profiling of all 20 CNGCs upon simulated herbivory revealed differential regulation of CNGCs (Supplemental Figure 1A, Supplemental Table 1), with CNGC19 being one of the highest expressed. We corroborated *CNGC19* gene expression upon *S. litura* feeding and found a similar trend of increase (Figure 1B). We looked at expression of *CNGC19* in systemic leaves as suggested by systemic Ca^{2+} elevation detected in Kiep et al. (2015). We found that *CNGC19* was upregulated in systemic leaves upon both W+W and W+OS treatments after 30 min (Figure 1C). The Arabidopsis *CNGC* gene family consists of 20 members divided into four main groups, namely I, II, III, and IV (IVa and IVb) as per their phylogenetic relationship (Mäser et al., 2001). *CNGC2* and *CNGC4* (involved in DAMP and R gene-mediated defense) are grouped to IVb, and *CNGC19* and *CNGC20* to IVa. Upon simulated herbivory, we found that *CNGC2* is upregulated in a delayed manner (at 60 min) by wounding and downregulated by W+OS treatment (Supplemental Figure 1B), *CNGC4* is not affected by either treatment and *CNGC20* is less induced in comparison to *CNGC19* with maximum 4.5-fold expression after 30 min (Supplemental Figures 1C and 1D). Hence *CNGC19* is a specific wound- and herbivory-activated gene in group IVa.

CNGC19 Is Expressed in Leaf Vasculature and Loss-of-Function Results in Increased *S. litura* Feeding

Because *CNGC19* is rapidly activated upon *S. litura* herbivory, we examined its site of expression in the leaf. *CNGC19* promoter activity was detected in primary, secondary, and tertiary veins and on wounding and *S. litura* herbivory, it also spread to leaf lamina (Figure 1D). We also detected its expression in trichome base cells (Figure 1D). To test the functional role of *CNGC19*, we compared the growth of *S. litura* larvae on wild type, *CNGC19* loss-of-function T-DNA lines (Supplemental Figures 2A and 2B) and *coi1-16* (positive control-JA receptor mutant). None of the plants tested had any developmental or growth defect phenotype. We observed that *S. litura* larvae feed on a larger leaf area and gain significantly more weight on the mutant *cngc19-2* (SALK_129200) and *cngc19-1* (SALK_027306) lines as compared with the wild type after 8 d (Figures 1E and 1F). The experiment was repeated three times showing significant differences by one-way ANOVA. Larvae feeding on *coi1-16* lines gain the most weight as the JA pathway is affected. The weight gain of *S. litura* larvae on *cngc19* mutants is due to decreased plant defense in the lines. By contrast, *S. litura* feeding on the closely related *cngc20* mutant did not alter leaf area eaten and weight of larvae over the wild-type control (Supplemental Figures 3A to 3C). Because cyclic nucleotides (cAMP/cGMP) are ligands that activate CNGCs, we measured their levels upon *S. litura* OS application and found that cAMP levels are elevated (Supplemental Figure 4A), which coincides with *CNGC19* expression at 2.5 min (Supplemental Figure 4B).

CNGC19 Is Crucial for Ca^{2+} Signal Propagation through the Vasculature

Because *CNGC19* is activated very rapidly upon herbivory, we wanted to understand its role in wound-induced Ca^{2+} signal generation in the local leaf. We employed the transgenic Ca^{2+} reporter, GCaMP3 (Toyota et al., 2018), and generated *cngc19*-mutant–expressing GCaMP3 by crossing *cngc19**GCaMP3 lines. In this study, a single leaf in a rosette was mechanically wounded and imaged. We used the whole local leaf for quantification (Supplemental Figure 5A) and both wild type and *cngc19* were selected for equal fluorescence levels (Supplemental Figure 5B). In wild type, the Ca^{2+} signals start near the wound site, move to vasculature, and then spread to the entire leaf lamina within 60 s (Figure 2A; Supplemental Movies 1 and 3). In *cngc19*, there is aberrant, misregulated, and reduced Ca^{2+} signal propagation through the vasculature. The Ca^{2+} signals do not spread to the entire leaf and are often found on one side of the leaf and with an irregular vascular route of propagation (Figure 2A; Supplemental Movies 2 and 4). The *cngc19* mutants have reduced Ca^{2+} elevation compared with the wild type upon wounding (Figure 2B). Hence, CNGC19 channel is crucial for wound-induced Ca^{2+} signal generation and propagation.

CNGC19 Is a Plasma Membrane-Localized Ca^{2+}-Permeable Channel

Several plant CNGCs have been shown to represent Ca^{2+}-permeable channels, but CNGC19 has not been characterized so far. A C-terminal YFP-tagged version of CNGC19 (CNGC19-YFP) was expressed in *Xenopus* oocytes and cAMP-induced currents recorded under a two-electrode voltage clamp (TEVC). CNGC19-YFP injected oocytes exhibited strong yellow fluorescence at their

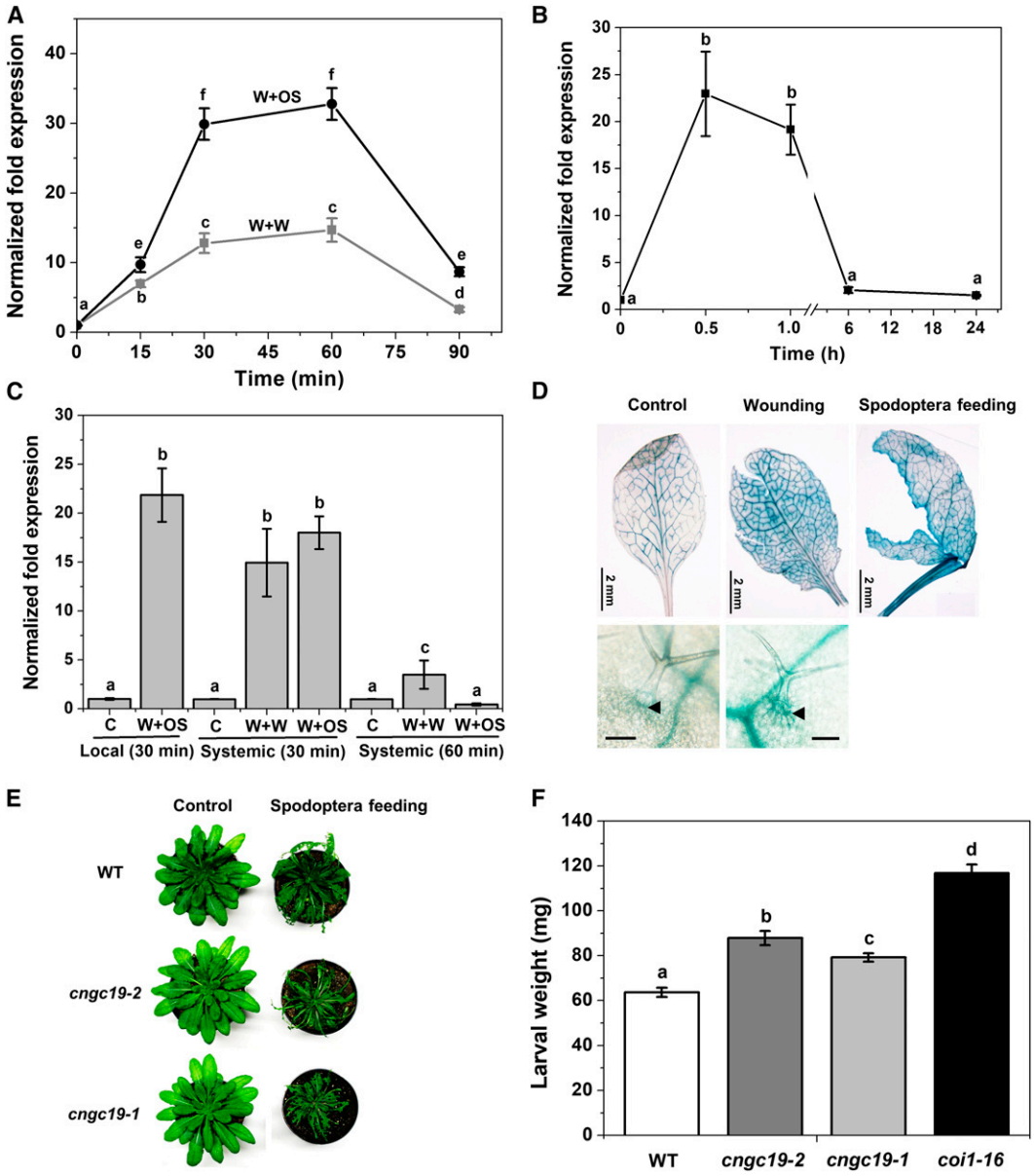

Figure 1. Spodoptera Herbivory-Induced *CNGC19* Transcript Elicitation in Local and Systemic Leaves and its Functional Role in Herbivory.

(A) *CNGC19* transcript levels in 6-week–old wild type Arabidopsis leaves treated with wounding+water (W+W) and wounding+*S. litura* OS (W+OS) for 15, 30, 60, and 90 min. Leaves were wounded with a pattern wheel and subsequently 20 μL of water or 1:1 diluted OS per leaf was applied. Gene transcript abundance was determined by real-time PCR; samples were normalized by plant *RPS18* mRNA. The graphs show fold change of mRNA level relative to untreated control. Fold change is the mean ± SE ($n = 4$) and experiments were duplicated with similar results. Different letters indicate statistically significant differences among samples, calculated by one-way ANOVA with a posthoc SNK test ($P \leq 0.05$). WT, wild type.

(B) *CNGC19* transcript levels in 6-week–old Arabidopsis local leaves after 0.5, 1, 6, and 24 h of *S. litura* feeding. Unfed plants were used as a control for the calculation. Plotted values are the mean ± SE ($n = 4$). Different letters indicate statistically significant differences among samples, calculated by one-way ANOVA with a posthoc SNK test ($P \leq 0.05$).

(C) *CNGC19* transcript levels in 6-week–old Arabidopsis systemic leaves after 30 and 60 min of W+W and W+OS application. Local leaf is leaf 8, while systemic leaves are a pool of vascular-connected leaf 5, 11, 13, and 16. Locally treated W+OS (30 min) was included as the positive control from the same set of plants. Plotted values = mean ± SE ($n = 4$) and are repeated twice independently. Different letters indicate statistically significant differences among samples, calculated by one-way ANOVA with a posthoc SNK test ($P \leq 0.05$).

(D) *CNGC19* promoter activity in leaf vasculature upon wounding and Spodoptera feeding. *ProCNGC19:GUS*-expressing transgenic plants were mechanically wounded by needle or fed on by Spodoptera (fourth-instar larvae). After 5 min of treatments, leaf tissues were collected and incubated in GUS staining solution for 1 h. Upper,panel indicates promoter activity in leaf and lower panel indicates, promoter activity in trichome base cells (Scale bar = 100 μm).

periphery, whereas water-injected oocytes did not show any fluorescence (Supplemental Figures 6A to 6C). A line scan shows that fluorescence is restricted to the boundary of the oocyte (Supplemental Figures 6B and 6D). TEVC experiments were performed on CNGC19-YFP-expressing oocytes, subjecting them to pulses ranging from −130 mV to +40 mV. Large inward currents were observed in CNGC19-YFP–expressing oocytes upon the addition of external $CaCl_2$ and dibutyryl cAMP (300 μM) on hyperpolarizing <−90 mV (Figures 3A iv and 3B). Addition of cAMP alone or $CaCl_2$ alone did not elicit currents, nor were currents seen in water-injected oocytes subject to both cAMP and Ca^{2+} (Figure 3A i, vi, and viii). The cyclic nucleotide gating of the channel is confirmed, as $CaCl_2$ alone does not produce inward current (Figure 3A vi), but subsequent addition of cAMP resulted in large inward currents (Figure 3A vii). *Xenopus* oocytes express a Ca^{2+}-activated chloride current that is activated on elevation of Ca^{2+}_{cyt}. Treatment with the Ca^{2+}-activated chloride current inhibitor, 4, 4′-diisothiocyanatostilbene-2, 2′-disulfonic acid disodium (DIDS; 300 μM), results in reduction of the Ca^{2+}-activated inward current (Figures 3A v to 3C). We also tested the ion selectivity of the channel using monovalent cations K^+ and Na^+, and near-background currents were observed upon their addition in the presence of cAMP (Figures 3A ii and iii to 3C). These data establish that CNGC19 is a Ca^{2+}-permeable channel.

Most CNGCs are reported to be plasma membrane proteins. However, vacuolar localization has been reported for CNGC19 in Arabidopsis protoplasts (Yuen and Christopher, 2013). To confirm the subcellular localization, we did a co-localization experiment using *Nicotiana benthamiana* transiently cotransformed with CNGC19-YFP and vacuolar and plasma membrane markers. In *N. benthamiana*, CNGC19 localized to the plasma membrane and overlays with PM-mCherry marker, but not with TP-mCherry (Figure 3D). According to Nelson et al. (2007) and Zhang et al. (2017a), one of the clear features of vacuolar localization is the presence of transvacuolar strands and separation of tonoplast from neighboring cells, which we see in TP-mCherry (arrow, Supplemental Figure 7A). We found that CNGC19 does not overlay with any of these features using TP-mCherry (arrows in Figure 3D and Supplemental Figure 7A). It also does not overlay with chlorophyll markers (Supplemental Figure 7B). Using protein gel blot, we detected full-length CNGC19-YFP protein expression (Supplemental Figure 7C). Hence, we conclude that CNGC19 is plasma membrane localized Ca^{2+} channel.

The CNGC19 Channel Is Involved in *At*Pep Perception

The herbivory-induced immune system is not exclusively based on detection of *S. litura* OS, but also on damaged self-damage/DAMPs that are released upon wounding (Boller and Felix, 2009; Albert, 2013). In Arabidopsis, a family of endogenous elicitor peptides referred to as "*At*Peps" acts as DAMP and amplifies the herbivory defense response (Huffaker and Ryan, 2007; Bartels et al., 2013). The Arabidopsis plasma membrane Pep-receptors, PEPR1 and PEPR2, perceive proteinaceous Peps (Yamaguchi et al., 2006, 2010; Krol et al., 2010). The Arabidopsis Pep-PEPR system is induced by Spodoptera feeding and is crucial for plant defense against herbivory (Klauser et al., 2015). Using ATTED-II, a plant coexpression database (http://atted.jp), we found that *CNGC19* coexpresses with *PEPR2* and *PEPR1* on the gene network (Figure 4A). *CNGC19* is wound- and OS-inducible upon simulated herbivory (Figure 1A) and we found that PEPR1 and PEPR2 coexpresses at similar time points (Figure 4B). CNGC19 (Figure 1D) and PEPRs (Bartels et al., 2013) are expressed in leaf vasculature. To assess the possible contribution of the PEPR pathway to herbivory-induced *CNGC19* induction, we analyzed *CNGC19* expression upon simulated herbivory in a *pepr1 pepr2* double mutant, which cannot sense Peps. We found that *CNGC19* is significantly downregulated in the absence of PEPRs upon both wounding and OS application at 30 min (Figure 4C), indicating it might be regulated/act downstream of PEPRs. At 60 min this effect is lost, suggesting that only at early time points *CNGC19* expression is PEPR-regulated. Because OS is a complex mixture of many HAMPs and DAMPs, its effect on cAMP levels in PEPR-receptor mutants remains similar (Supplemental Figure 8). Hence, we examined whether Pep-induced Ca^{2+}elevation was altered in *cngc19*. Ca^{2+} elevation with Pep1 treatment was reduced in *cngc19* compared with wild type at all time points (Figure 4D), indicating a role for CNGC19 channel in generating the Pep-induced Ca^{2+} elevation. It was previously known that Pep1 application induced cytosolic Ca^{2+} elevation in Arabidopsis via CNGC2 (Ma et al., 2012). We further hypothesized that CNGC19 might interact with PEPR and the coreceptor BAK1 on the plasma membrane. To test this hypothesis, we performed a split-ubiquitin assay as all of these proteins are plasma-membrane associated. Full-length CNGC19 and PEPR1, and PEPR2 and BAK1 proteins, were expressed as C-terminal ubiquitin (Cub) or N-terminal ubiquitin (Nub) fusions in yeast, respectively. After mating, the presence of the plasmids was verified by growth of yeast cells on synthetic complete medium containing Ade and His (SC+AH). CNGC19-Cub fusions showed no complementation with PEPR1-Nub, PEPR2-Nub, or BAK1-Nub (Figure 4E), indicating lack of pairwise interactions. CNGC19-Nub wild type interaction with CNGC19-Cub was used as a positive control due to the fact that NubWt spontaneously reassembles with Cub. We also confirmed the data with BiFC that CNGC19 does not interact with PEPR1, PEPR2, and BAK1 proteins in planta (Supplemental Figure 9). CNGC19 is thus an important Ca^{2+} channel involved

Figure 1. (continued).

(E) and **(F)** Larval weight after feeding on Col-0, *coi1-16* and two different *cngc19* lines, *cngc19-2* (SALK_129200) and *cngc19-1* (SALK_027306). Phenotype and leaf area eaten upon feeding of *S. litura* larvae on Col-0 and *cngc19* mutant lines. For all experiments, *S. litura* first-instar larvae growing in light for 3 d after hatching were preweighed and three larvae were placed on plants of each genotype. The larval weight (mean ± SE) was measured after 8 d of feeding. Values are the mean of three independent experiments ($n = 85$). Statistically significant differences between larvae fed on Col-0 and *cngc19* mutant lines were analyzed by one-way ANOVA with a post-hoc SNK test ($P \leq 0.001$). WT, wild type.

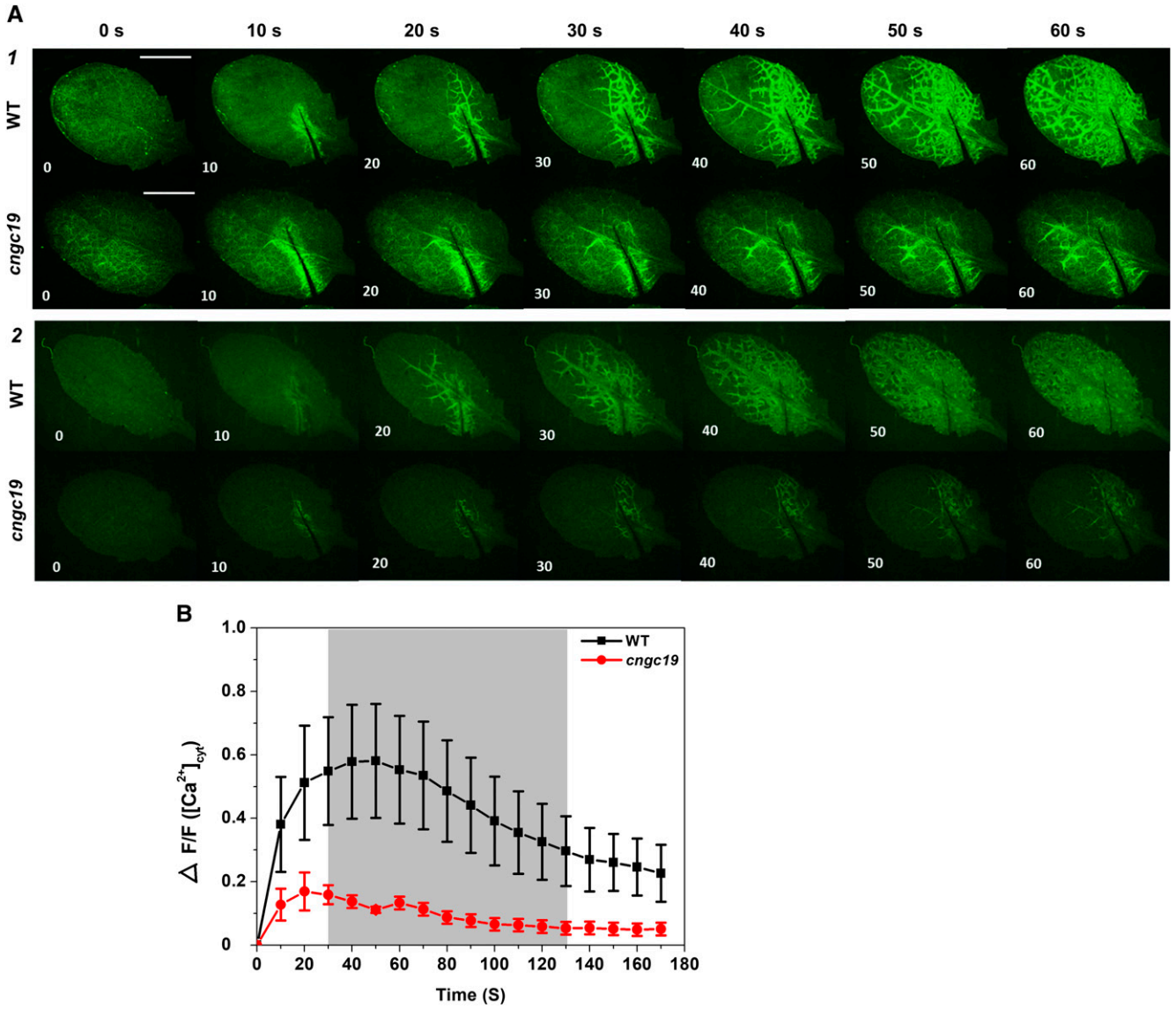

Figure 2. Wound-Induced Cytosolic Ca^{2+} Levels in Local Leaves of Wild Type and *cngc19* Mutant.

(A1) and **(A2)** Representative stereomicroscope images showing fluorescence upon wounding at 10-s intervals in wild type and *cngc19-2*. Cutting leaf 5 in a 4-week–old plant caused a local Ca^{2+}_{cyt} increase that propagated within the leaf. Frame A1 is from Supplemental Movie 1 (wild type) and Supplemental Movie 2 (*cngc19*); frame A2 is from Supplemental Movie 3 (wild type) and Supplemental Movie 4 (*cngc19*) with linear brightness-contrast correction. $n > 7$ in independent experiments. Scale bar = 5 mm.

(B) Mean of normalized fluorescence intensity $\Delta F/F$ of wild type (black) and *cngc19-2* (red) at 10-s intervals after wounding the leaf with fine scissors. F, average fluorescence intensity before wounding (baseline); ΔF, difference between measured fluorescence and baseline fluorescence (ΔF = fluorescence after wounding − baseline fluorescence). The entire leaf area was selected for calculating $\Delta F/F$ (Supplemental Figure 5). Error bars represent the SE of the mean ($n = 8$). Gray shading indicates a significant difference using 2-tailed Student's t-test at $P \leq 0.05$. WT, wild type.

in perception of DAMP (Pep) and is regulated by PEPR during the early stages of herbivory.

CNGC19 Is Jasmonate-Regulated and Loss-of-Function Affects Jasmonate Signaling upon Herbivory

The plant hormone JA and its derivatives are key players in the regulation of induced plant defense against a wide range of herbivorous insects (Gfeller et al., 2011). Because the kinetics of *CNGC19* expression (at 30 to 60 min) overlaps with herbivory-induced jasmonate biosynthesis (Vadassery et al., 2012), we hypothesized that *CNGC19* upregulation might be regulated via phytohormones. To answer this question, *CNGC19* expression under JA-Ile (bioactive form of jasmonate) treatment was studied. *CNGC19* expression was transiently induced with a maximum of ninefold after 30 min of JA-Ile treatment; *LOX2* upregulation was

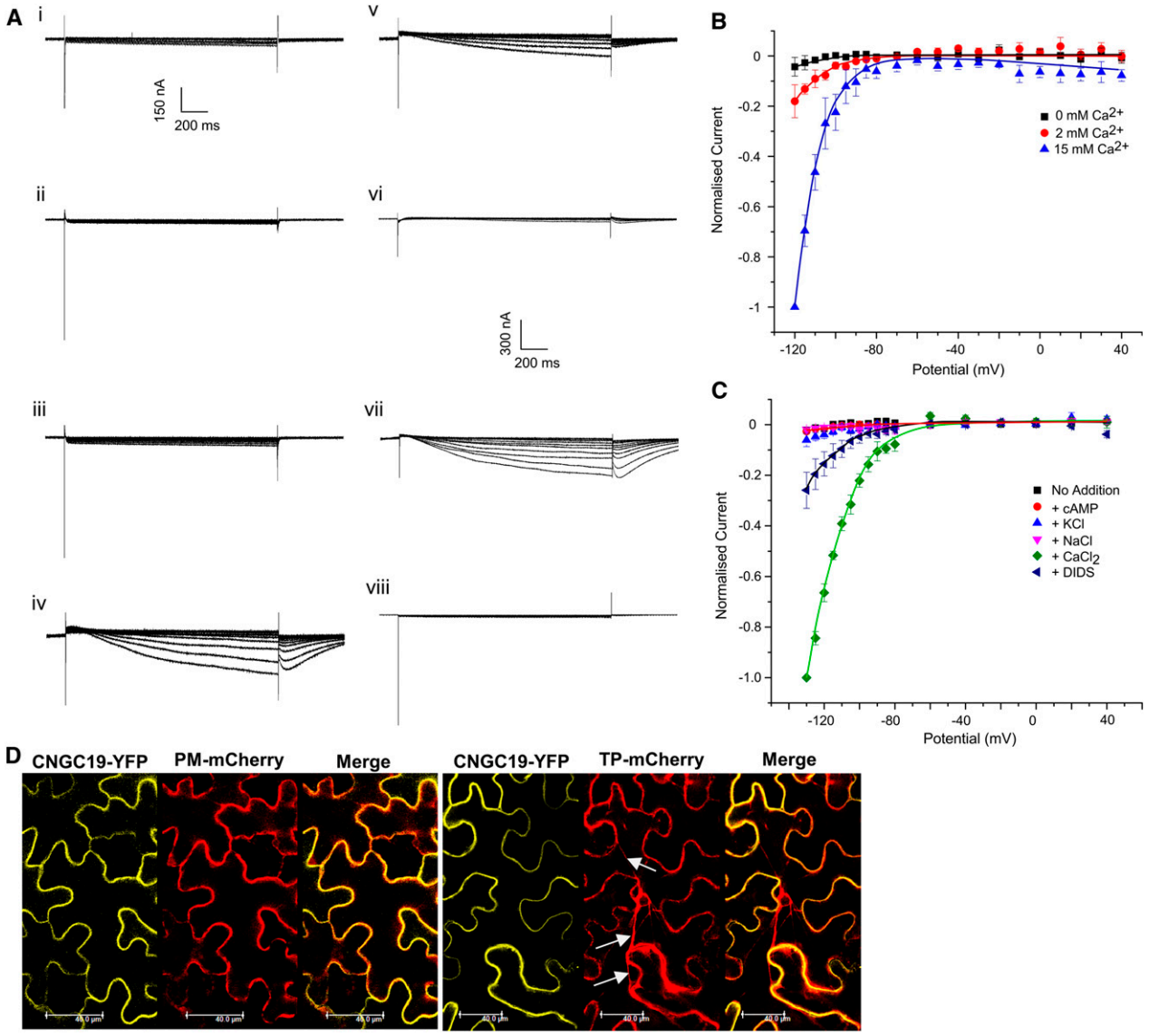

Figure 3. CNGC19 Is a Plasma-Membrane–Localized Ca^{2+}-Permeable Channel.

(A) CNGC19-YFP–expressing *Xenopus* oocytes show inward rectifying currents. Oocytes were held at −60 mV and stepped to a range of potentials from −120 mV to +40 mV. Traces (i) to (v) were acquired sequentially on one oocyte and no washout was performed for recordings. Currents were recorded after the addition of (i) 300-μM dibutyryl-cAMP and incubation for 15 min; followed by (ii) 10-mM NaCl, (iii) 10-mM KCl, (iv) 15-mM $CaCl_2$, and (v) 300-μM DIDS. A separate oocyte was subjected to the same voltage pulse protocol with the following additions sequentially (and no washout was performed for recordings): (vi) $CaCl_2$ alone; (vii) after a further addition of 300-μM dibutyryl cAMP and incubation for 15 min ($CaCl_2$+cAMP). (viii) A water-injected oocyte to which 300-μM dibutyryl cAMP has been added, incubated for 15 min and then 15-mM $CaCl_2$ added (negative control). Currents at −120 mV in these oocytes were of the order of 10 nA, whereas those in the corresponding CNGC19-expressing oocytes ranged from −400 to −1,400 nA. Note that traces (i) to (v) are from one oocyte, with salt solutions and DIDS being added in the presence of cAMP. Traces (vi) and (vii) are from a second oocyte, both expressing CNGC19-YFP. Traces in (viii) are from a third oocyte not expressing CNGC19-YFP, which was instead injected with water.

(B) Plot of currents recorded from CNGC19-YFP-injected oocytes incubated with 300-μM dibutyryl cAMP in the presence of 0 mM (■), 2 mM (●) or 15 mM (▲) $CaCl_2$ over a range of potentials from −120 mV to +40 mV. All data for an oocyte were normalized to the current recorded from that oocyte at −120 mV in the presence of Ca^{2+}. Data = mean ± SE for six oocytes.

(C) Plot of currents recorded from CNGC19-YFP injected oocytes at potentials ranging from −130 mV to +40 mV. Oocytes in recording buffer (■); with 300-μM dibutyryl cAMP (●); 10-mM KCl (▲); 10 mM NaCl (▼); 15-mM $CaCl_2$ (◆); 300-μM DIDS (◇). All data for an oocyte were normalized to the current recorded from that oocyte at −130 mV in the presence of Ca^{2+}. Data = mean ± SE for six oocytes.

(D) Visualization of CNGC19-YFP full-length fusion protein in transiently transformed *N. benthamiana* using confocal laser scanning microscopy. Plasma membrane marker PM-mCherry and tonoplast marker TP-mCherry were coinfiltrated to facilitate CNGC19-YFP subcellular localization. White arrows indicate transvacuolar strands in TP-mCherry. Scale bar = 40 μm.

used as a marker for treatment (Figure 5A). To establish whether *CNGC19* expression is dependent on the JA-Ile receptor, COI1, after herbivory, we analyzed its expression in wild-type and homozygous *coi1-1* plants after simulated herbivory. *CNGC19* expression was less upregulated upon both W+W and W+OS treatments in the *coi1-1* mutant at all time points, suggesting a role in regulating *CNGC19* transcription (Figure 5B). To determine whether the increased insect performance on *cngc19* is due to altered phytohormone levels, both wild type and *cngc19-2* were challenged with Spodoptera larvae and phytohormones were measured at different time points. The levels of JA and JA-Ile increased in wild type upon Spodoptera feeding. By contrast, the *cngc19-2* mutant showed a reduced level of JA and JA-Ile when compared with the wild type after herbivory (Figures 5C and 5D). We found similar results with *cngc19-1* line (Supplemental Figure 10A). Both mutants, *cngc19-1* and *cngc19-2*, also show significantly reduced expression of the JA-responsive genes *VEGETATIVE STORAGE PROTEIN2*, *THIONIN2.1*, *PLANT DEFENSIN1.2*, and *LOX2* compared with wild type upon herbivory (Figure 5E). SA content was similar in both wild type and *cngc19* mutants (Supplemental Figures 10B and 10C). In conclusion, the loss-of-function of *CNGC19* affects the jasmonate accumulation upon herbivory, contributing to reduced defense.

Aliphatic GS Levels Are Constitutively Downregulated in *cngc19* Mutants with Overaccumulation of the Biosynthetic Precursor Methionine

Downstream of jasmonate signaling, secondary metabolites play a key role in Arabidopsis-induced defense against herbivory. GSs are important secondary metabolites involved in resistance to generalist insects (Müller et al., 2010). We wanted to evaluate the influence of loss-of-function of *CNGC19* on GS accumulation to see if this could further explain increased *S. litura* herbivory. We analyzed the basal GS content of *cngc19* mutants and wild-type rosettes. The *cngc19* mutants have greatly reduced accumulation of total GS when compared with wild type. The decrease in total GSs was due to a drastic reduction of aliphatic rather than indolic GS content in *cngc19* mutants (Figure 6A; Supplemental Table 2). We further wanted to investigate the effects of *S. litura* feeding for 24 h on GS levels of wild type and *cngc19* mutants. The total GS levels increased upon Spodoptera feeding in the wild type and mutant; however, the GS levels in *cngc19* mutants were always lower than in wild type (Figure 6B). As seen in uninduced plants, we found that aliphatic GS levels remained lower in *cngc19* mutants than the wild type upon herbivory (Figure 6C). Spodoptera feeding resulted in an equal increase of indolic GS in both the wild type and *cngc19-2* line, and in the *cngc19-1* line, herbivory did not induce indolic GS (Figure 6D). Thus, in *cngc19* mutants, aliphatic GS levels are reduced under both basal and herbivory-induced conditions, hinting at perturbations in its biosynthesis.

To determine if metabolites other than GSs were altered upon *CNGC19* loss-of-function, we compared alterations in metabolites between *cngc19* and the wild type. However, we did not detect any metabolite changes apart from Met alterations. Aliphatic GS are derived from Met (Kliebenstein et al., 2001), and indeed, in whole rosette leaves, compared with wild type, the level of free Met was increased in *cngc19* mutants (Figure 7A). To identify if the excess Met is transported out in the form of s-methyl Met (SMM, the main transport form of Met), its levels were also measured. The SMM levels were higher in *cngc19* mutants compared with wild type, confirming transport of excess Met (Figure 7B). This elevation in free Met and its transport derivative, SMM, support the conclusion that *cngc19* mutants are defective in the conversion of Met to aliphatic GS. We looked at the expression profiles of all genes involved in aliphatic GS biosynthesis (Burow et al., 2015) in wild type and *cngc19* mutants, and found that *BCAT4* was highly reduced in both mutants (Figure 7C). The first process of Met chain elongation in the biosynthesis of aliphatic GSs is the deamination of Met to the corresponding 2-oxo acids by a branched-chain amino acid aminotransferase (BCAT). BCAT4 showed high efficiency to Met, and is involved in the first part of the biosynthesis of Met-derived aliphatic GSs (Schuster et al., 2006). *A. thaliana* possesses six branched-chain transaminase (BCAT1 to 6). An expression profiling in wild type and *cngc19* mutants revealed that the expression of *BCAT4* was most highly reduced in *cngc19* mutants (Figure 7D). *BCAT2* and *BCAT1* expression was also downregulated; however, neither of these genes are not involved in GS biosynthesis (Figure 7D). We further wanted to confirm that *BCAT4* has a functional role in *S. litura* herbivory, and therefore a feeding assay with loss-of-function mutant *bcat4* was done. We found that the *bcat4* mutant with highly reduced aliphatic GS shows decreased defense as insects gain more weight and eat a larger leaf area, similar to *cngc19* (Figure 7E). Interestingly, *ProBCAT4*:*GUS* lines show increased activity in primary, secondary, and tertiary veins upon wounding and *S. litura* herbivory, similar to CNGC19 (Figure 7F).

CNGC19 Regulates Defense, Transport, Hormone, and Biotic Stress Genes upon Herbivory

To identify which other signaling pathways are regulated by CNGC19 upon herbivory, global transcript profiling was done using microarray in *cngc19* and wild-type plants after 1 d of *S. litura* feeding. Microarray indicated that 339 genes were upregulated and 347 genes were downregulated in *cngc19* compared with wild-type plants after 1 d of *S. litura* feeding (Supplemental Data Set). Gene ontology (GO) classification of the 686 up- or down-regulated genes revealed that they are mostly stress-regulated with five major functional categories of response to stimuli (18%), chemical stimuli (10%), transport (9.32%), light (3.54%), and wounding (1.49%), being highly enriched in the microarray (Figure 8A). The most differentially regulated 80 genes and GO-enriched gene list are depicted by heat map (Figure 8B; Supplemental Figure 11). We further tried to functionally annotate the genes using MapMan (v3.5.1; https://mapman.gabipd.org/) categorization and the selected genes were phytohormone-regulated genes (LOX, SnRK2.7, PP2A, and ERF), transporters of amino acids and nutrients (AMT1.5, PHT1.7, and AAP), defense-regulated genes (RIN4-like protein, defensins, MOS7, and RRS1), receptor kinases (LRR1, CRK/DUF27, BSK9), MAPK pathway genes (MPK12, MEKK1, WRKY55, and MKK8), and glutamate receptors (GLR2, GLR3.5, and GLR3.6; Figure 8C; Supplemental Data Set). Thus, loss-of-function of *CNGC19* deregulates early signaling pathway related to plant defense.

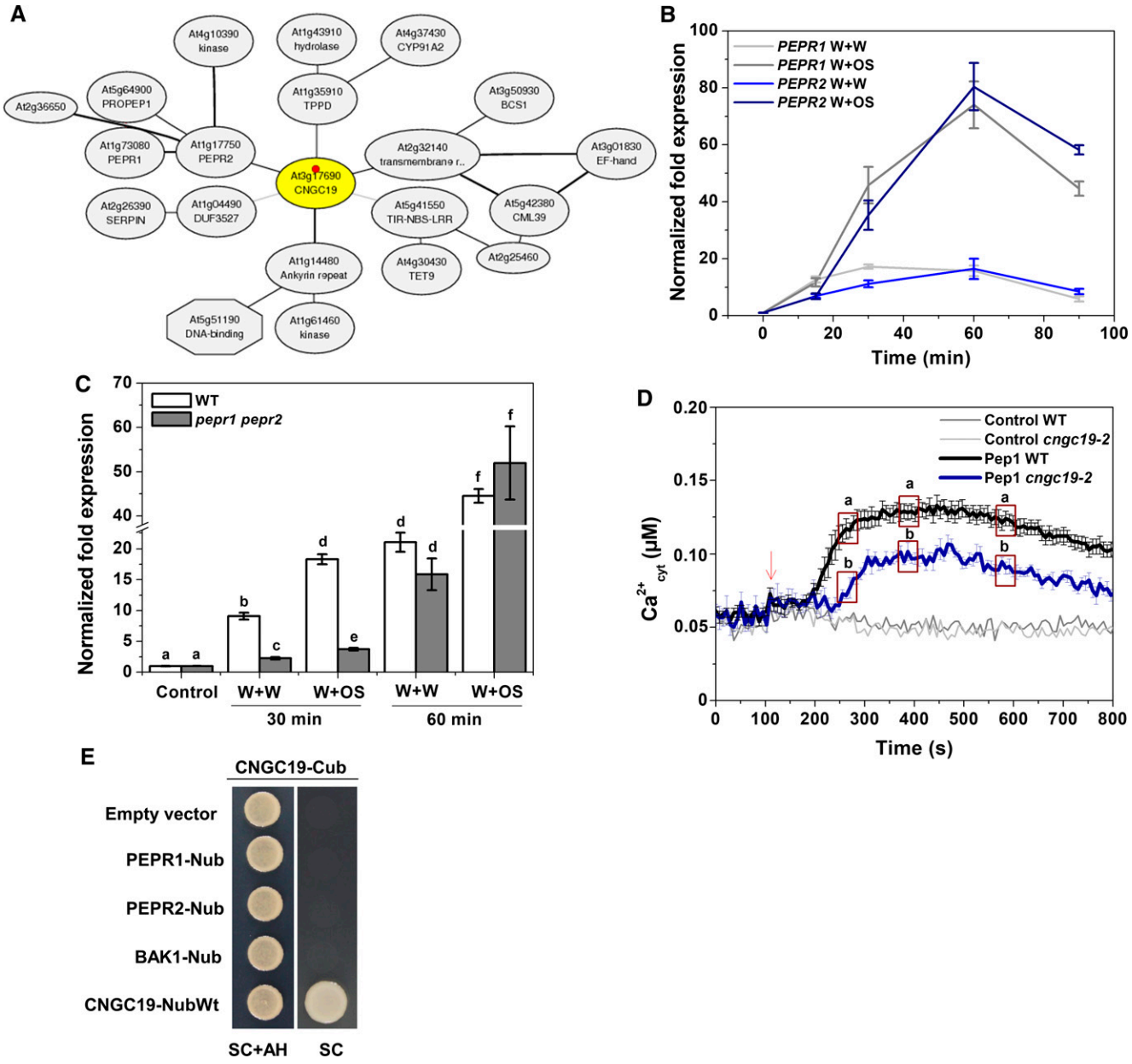

Figure 4. *CNGC19* Expression Is PEPR-Regulated upon *S. litura* Herbivory and Is Involved in the Generation of Ca^{2+} Signatures upon Pep1 Perception.

(A) *CNGC19* coexpression network according to ATTED-II, a plant coexpression database (http://atted.jp).

(B) *PEPR2* and *PEPR1* transcript levels in 6-week–old Arabidopsis leaves treated with *S. litura* OS for 15, 30, 60, and 90 min. Leaves were wounded with a pattern wheel and subsequently 20 µL of water or 1:1 diluted OS per leaf was applied. Gene transcript abundance was determined by real-time PCR, and samples were normalized by plant *RPS18* mRNA. The graphs show fold change of mRNA level relative to untreated control. Fold change is the mean ± SE (n = 4) and experiments were duplicated with similar results.

(C) *CNGC19* transcript levels in 6-week–old wild-type and *pepr1 pepr2* leaves treated with W+W and W+OS. Gene transcript abundance was determined by real-time PCR, and samples were normalized by plant *RPS18* mRNA. The graphs show mean ± SE (n = 4) fold change of mRNA level relative to the respective untreated control. Statistically significant differences between wild-type and *pepr1 pepr2* plants were analyzed by one-way ANOVA with a posthoc SNK test ($P \leq 0.05$).

(D) Elevation in cytosolic Ca^{2+} concentration (Ca^{2+}_{cyt}) in 10-day–old wild type (Aeq) and *cngc19-2-pMAQ2* seedlings (n = 5), by treatment with 20-nM Pep1. Arrow indicates stimulation by Pep1 treatment. Water was used as a control and gave background readings (light and dark gray lines). The experiment was repeated three times with similar results and the figures are representative data from one experiment. Three random sets of five data points were analyzed for statistically significant differences between wild type (Aeq) and *cngc19-2-pMAQ2* by one-way ANOVA with a posthoc SNK test ($P \leq 0.05$).

CNGC19 Interacts with *S. litura*-Induced CaM2 In Planta

The carboxyl tail of several plant CNGCs has been shown to bind to CaM in a Ca^{2+}-dependent manner and regulate the closing and opening of the channel. CNGC20, a Group IVa member, is known to interact with CaMs rather than with CaM-like proteins (CMLs; Fischer et al., 2013). The Arabidopsis genome contains seven CaM genes encoding four different isoforms that are highly conserved—CaM1/CaM4, CaM2/CaM3/CaM5, CaM6, and CaM7 (McCormack and Braam, 2003). Hence, to identify the downstream interaction partner of CNGC19, the CNGC19 C terminus was tested for interaction with each of the four Arabidopsis CaM isoforms by yeast two hybrid (Y2H). Fischer et al. (2017) had shown with Y2H that CNGC19 interacts with CaM2, CaM4, CaM6, and CaM7. We were able to show that CNGC19 interacts with CaM2, CaM3, CaM6, and CaM7 in SD-*Leu*/-*Trp*/-*His* (TDO) and QDO plates (Figure 9A; Supplemental Figure 12A). The presence of the inhibitor of the HIS reporter gene, 3-amino-1, 2, 4-triazole (3-AT), reduced yeast growth to differing extents, revealing strong CaM–CNGC19 interaction (Supplemental Figure 12A). We also tested in planta interaction of CaMs with CNGC19 using BiFC and found that CaM2, CaM3, CaM6, and CaM7 interact with CNGC19, confirming the Y2H (Figure 9B; Supplemental Figure 12B). As a negative control, we used CML42, which was previously shown to be involved in herbivory but shows no interaction with CNGC19 in Y2H or in BiFC (Supplemental Figures 12A and 12B). To identify which interacting CaMs are regulated upon herbivory and hence crucial, we conducted an expression analysis using simulated herbivory. We found that *CaM2* was most highly upregulated by wounding and OS application (Figure 9C; Supplemental Figure 13). Because CNGC19 interacts with CaM2, we tested loss-of-function of *CaM2* for a functional role in herbivory. The *cam2* mutant shows increased *S. litura* feeding, indicating a breakdown of plant defense (Figure 9D). We thus show that herbivory-induced CNGC19 and CaM2 interact in planta and this activates downstream defense signaling.

DISCUSSION

The Ca^{2+}-Permeable Channel *CNGC19* Is Integral for Herbivory-Activated Ca^{2+} Signaling

In this study, we uncovered the role of a novel calcium channel, CNGC19, in plant perception of herbivory. Upon *S. litura* herbivory, unknown receptors perceive wounding and HAMPs/DAMPs and activate a plasma membrane-localized, cyclic nucleotide-gated, Ca^{2+}-permeable channel, CNGC19. Ca^{2+} influx into the local attacked leaf activates downstream defense signaling. Loss of CNGC19 results in increased *S. litura* herbivory and breakdown of plant defense (Figure 10). Wound-induced intravascular Ca^{2+} fluxes in the attacked leaf require CNGC19 function. *CNGC19* is a late-activated salt-responsive gene, known to be expressed constitutively in root phloem and shoot vasculature; however, no functional role of *cngc19* upon salt stress has been reported in Kugler et al. (2009). The observation that Ca^{2+} signals are not completely abolished in *cngc19* leads us to conclude that wound-induced Ca^{2+} signal generation might be controlled by additional genetic interactions between CNGCs and unknown transporters (Figure 10).

Plants respond rapidly to insect herbivory with electrical signals and elevation of Ca^{2+}_{cyt} in the cytosol near the damage site or distal/systemic to it (Mousavi et al., 2013; Kiep et al., 2015). CNGC19 is needed for optimal vasculature-based spread of Ca^{2+} signals in the local leaf. We have previously shown that the vacuolar ion channel, TPC1, is important for the generation of a systemic Ca^{2+} response, but not for local elevation of Ca^{2+}_{cyt} upon herbivory (Kiep et al., 2015). Mutations in the GLR proteins (GLRs 3.1, 3.3, and 3.6) strongly reduced wound-induced electrical and Ca^{2+} signaling (Mousavi et al., 2013; Nguyen et al., 2018; Toyota et al., 2018). The axial and radial distributions of systemic Ca^{2+}_{cyt} fluxes are differentially affected in each *glr* mutant, with *glr3.6* exhibiting severe reduction. The systemic Ca^{2+}_{cyt} signal propagation, which is completely inhibited in the *glr3.3 glr3.6* double mutant, is restored to nearly wild-type levels by driving GLR3.6 expression in the double mutant line (Toyota et al., 2018). In *glr3.3*, the systemic Ca^{2+} signal is weaker, and exclusively vascular, compared with the signal from the wild type, *glr3.1*, and *glr3.6*, in which some perivascular Ca^{2+}_{cyt} signals are present (Nguyen et al., 2018). GLR3.3 and GLR3.6 have not experimentally been shown to form Ca^{2+}-permeable channels. Moreover, the role of GLRs in local leaf Ca^{2+}_{cyt} elevation has not been studied intensively, in part due to wounding methods aimed at addressing systemic Ca^{2+} signal generation after petiole clipping (Toyota et al., 2018) and crush wounding of half the leaf (Mousavi et al., 2013). Upon crush wounding, single mutant *glr3.3* and double mutant *glr3.3 glr3.6* displayed a generalized reduction in Ca^{2+} signals in the local leaf (Nguyen et al., 2018), but no aberrant distribution of Ca^{2+} signal through the vasculature as in the case of *cngc19*. Surprisingly, systemic Ca^{2+}_{cyt} signals and a functional role against herbivory appear to be regulated differentially. Among the single mutants of *glr3.1*, *glr3.3*, and *glr3.6*, the insects gained weight only on *glr3.3*, indicating a major role for this gene among the GLRs. Among the double mutants tested, insects gain more weight on *glr3.1 glr3.3* than on the well-characterized *glr3.3 glr3.6*, indicating that final defense output is much more complex than loss of systemic Ca^{2+} elevation (Nguyen et al., 2018). CNGC19 had both altered local Ca^{2+} elevation and a functional phenotype upon herbivory. Phloem sieve elements (*GLR3.3* expression) and xylem contact cells (*GLR3.6* expression) function together for leaf-

Figure 4. (continued).

(E) CNGC19 full-length protein was fused with Cub and other proteins (PEPR1, PEPR2, and BAK1) were fused with Nub. CNGC19 and other constructs were transformed in mating yeast strains THY.AP4 and THY.AP5, respectively. Both strains were mated in Yeast extract-Peptone-Dextrose medium and then plated on SC+AH- and SC-medium–containing plates to assess the interaction. Empty Nub vector and CNGC19 fused with NubWt served as the negative and positive controls for the experiment, respectively.

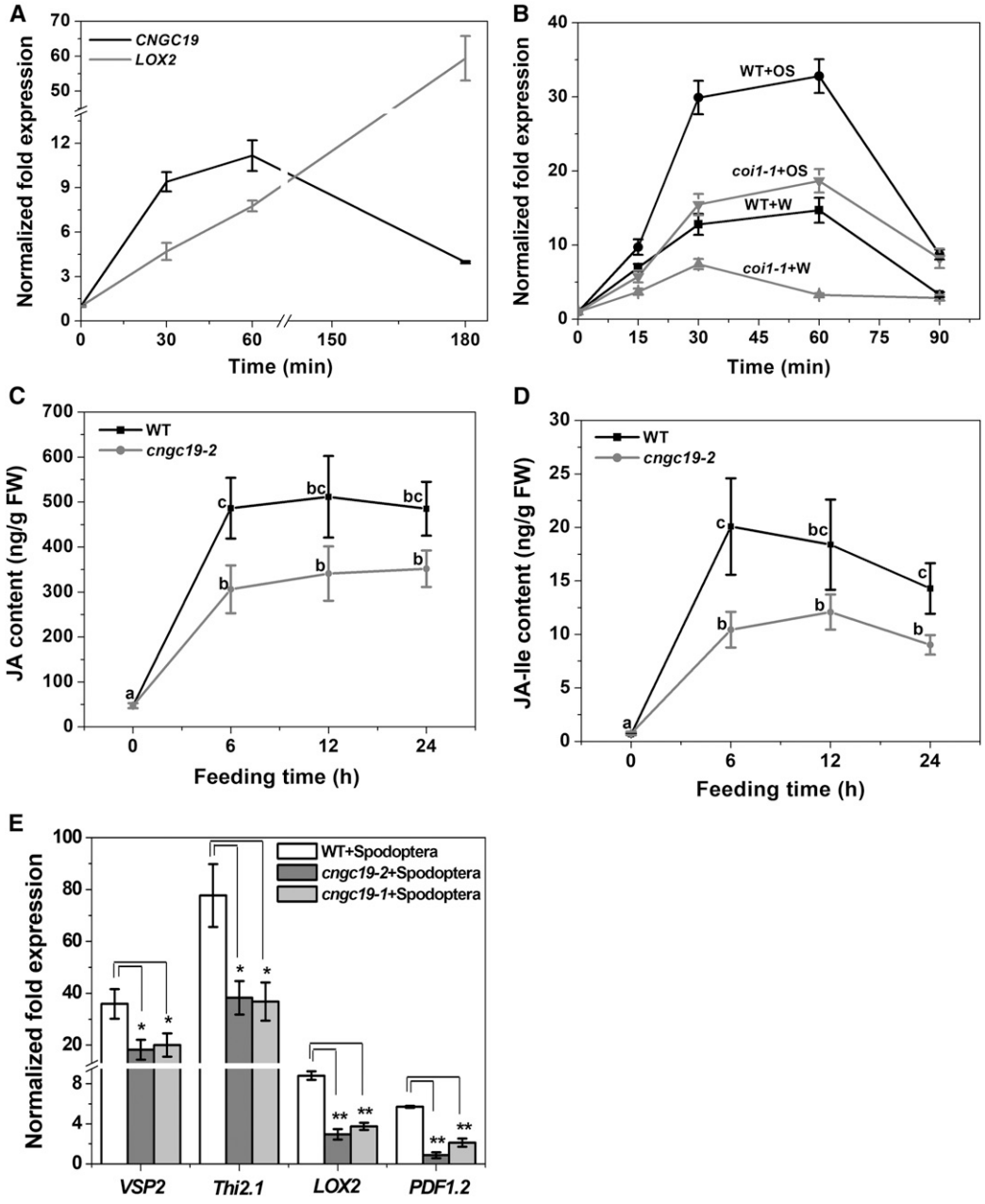

Figure 5. *CNGC19* Loss-of-Function Affects Jasmonate-Based Plant Defense.

(A) *CNGC19* transcript accumulation in 14-day–old Arabidopsis seedlings treated with 500-μM JA-Ile. The *LOX2* transcript was evaluated as a positive control for JA treatment. Values are mean ± SE ($n = 4$).

(B) *CNGC19* transcript accumulation in 6-week–old wild type (black) plant and JA perception mutant, *coi1-1* (gray) upon W+W and W+OS treatment. Gene transcript abundance was determined by real-time PCR, samples were normalized by plant *RPS18* mRNA. The graphs show mean ± SE ($n = 4$) fold change of mRNA level relative to respective untreated control. WT, wild type.

(C) and **(D)** JA **(C)** and JA-Ile **(D)** phytohormone elevation upon herbivory in *cngc19-2* mutant plants. Mean ± SE ($n = 18$) values are shown for JA, its bioactive form (+)-JA-Ile in Arabidopsis wild-type (black) and *cngc19-2* (gray) plants fed on by Spodoptera (fourth-instar larvae) for 6, 12, and 24 h. The phytohormone levels were measured from local wounded leaves in the plant rosette. Values are means of six independent experiments. Statistically significant differences between wild-type and *cngc19-2* plants were analyzed by one-way ANOVA with a posthoc SNK test ($P \leq 0.05$). WT, wild type.

(E) Mean ± SE ($n = 4$) relative mRNA levels of defense-related genes *VEGETATIVE STORAGE PROTEIN2* (*VSP2*), *THIONIN2.1* (*Thi2.1*), *LOX2*, and *PLANT DEFENSIN1.2* (*PDF1.2*), in Spodoptera-infested leaves of wild-type (white), *cngc19-2* (dark gray), and *cngc19-1* (light gray) plants. Spodoptera (fourth-instar larvae) fed on wild-type and both *cngc19* lines for 6 h. Undamaged plants served as controls. Statistically significant differences between plants were analyzed by unpaired *t* test: $^{*}P \leq 0.05$; $^{**}P \leq 0.001$. WT, wild type.

to-leaf electrical signaling in a wounded plant (Nguyen et al., 2018). The CNGC19 expression pattern is very similar to *GLR3.3*, which is also expressed in leaf vasculature (phloem sieve elements) and trichome base cells (Nguyen et al., 2018). It is tempting to speculate that GLR3.3 might form protein complexes with CNGC19 for Ca^{2+} signal generation in the local leaf. From our study and other reports, it is clear that local and systemic Ca^{2+}_{cyt} elevations in response to wounding have different mechanistic bases and could involve parallel pathways involving multiple ion channels, consistent with the diversity of DAMPs/HAMPs generated upon herbivory. Our observation that CNGC19 is critical for wound-induced Ca^{2+} signal generation introduces a novel ion channel in defense activation.

Plant genomes do not encode canonical ion channels with Ca^{2+}-selective filters as found in the case of animals, but they do express ion channels that are permeable to Ca^{2+} and conduct currents (Demidchik et al., 2018). Cyclic nucleotide-gated channels, including CNGC 7 to 10, and CNGC14 and 16, have previously been shown to pass Ca^{2+} as part of a cation-selective current when expressed in heterologous cells (Zhou et al., 2014; Gao et al., 2016; Zhang et al., 2017b). Ca^{2+}-activated inward currents were activated upon hyperpolarization of CNGC19-expressing *Xenopus* oocytes in the presence of both cAMP and high external Ca^{2+}. Na^+ and K^+ did not show inward currents in the presence of cAMP in *Xenopus* oocytes expressing CNGC19-YFP. In the absence of a plot of reversal potential against the concentration of external cations, it is not possible to make a definitive statement about the selectivity of the channel. The very rapid deactivation of DIDS-insensitive tail currents (Figure 3A v) precluded attempts to measure reversal potentials accurately. The absence of K^+- or Na^+-induced inward currents and the steep dependence of this on external Ca^{2+} concentration is thus consistent with CNGC19 encoding a cyclic-nucleotide gated ion channel that is permeable to Ca^{2+}. Interestingly, the CNGC19 activation upon hyperpolarization strongly suggests the involvement, in planta, of an electrical long-distance signal, the so-called "system potential," which is initiated by wounding and herbivory (Zimmermann et al., 2009, 2016). CNGC19 might thus represent the first identified channel that responds to feeding-induced system potential. We report that CNGC19 is localized in planta to the plasma membrane and not to vacuoles, in contrast with the findings of Yuen and Christopher (2013), who reported CNGC19 and CNGC20 to be vacuolar-localized. Intriguingly, CNGC20 has also been shown to be localized to the plasma membrane (Fischer et al., 2013). However, our study does not rule out the possibility of sorting *CNGC19* along with other interacting proteins to internal Ca^{2+} reservoirs (ER, vacuole, and mitochondria) upon herbivory. GLRs interact with CORNICHON HOMOLOG proteins and are redistributed to other Ca^{2+} storing compartments inside plant cells that regulate Ca^{2+} signaling in pollen tube Ca^{2+} homeostasis (Wudick et al., 2018).

The Pep-PEPR pathway serves to intensify and/or propagate defense signaling after HAMP perception. The Arabidopsis Pep–PEPR system is induced by herbivore feeding and contributes to JA-mediated plant defense against herbivory (Klauser et al., 2015). PEPRs are localized to leaf vasculature, like CNGC19 (Klauser et al., 2015), and regulate *CNGC19* expression upon herbivory. The channel is also involved in generating the Pep-induced Ca^{2+} signature. The putative guanylyl cyclase (GC) domain within the PEPR1 receptor is suggested to provide the cGMP that stimulates CNGC2 channel opening upon Pep perception (Qi et al., 2010). However, we found that Spodoptera OS activates cNMP production to similar levels in wild-type and *pepr1 pepr2* mutants. Wounding, HAMPs, DAMPs, and unidentified elicitors in OS, might activate distinct receptors that could directly (via the presence of GC/AC domains) or indirectly (via posttranslational modifications) activate CNGCs (Figure 10). Hence PEPRs might only be involved in sensing the *At*Peps present in the crude OS or could interact with unknown receptors/phosphorylate targets. The role of CNGC19 in Pep-induced Ca^{2+} elevation hints at the formation of multiprotein complexes with CNGC2 to sense Peps.

CNGC19-Mediated Plant Defense upon Herbivory Is Controlled via JA-Ile Signaling

Plants rapidly activate biosynthesis of JA and JA-Ile to high levels on sensing herbivore attack. JA-Ile facilitates JAZ repressor binding to the COI1 jasmonate receptor and their subsequent ubiquitination, thereby activating jasmonate signaling (Sheard et al., 2010). Ca^{2+} is involved in the regulation of JA biosynthesis and signaling (Vadassery et al., 2012, 2014; Wasternack and Hause, 2013; Scholz et al., 2014). Herbivory-induced expression of *CNGC19* is COI1-dependent and feedback through the JA-Ile pathway might regulate it. The *cngc19* mutants had reduced levels of JA and JA-Ile after *S. litura* feeding. Downregulation of specific JA-responsive genes was observed in *cngc19* mutants. Thus, reduced activation of the jasmonate pathway contributes to decreased defense in *cngc19*. CNGCs have not previously been shown to have a role in jasmonate signaling except in *dnd* mutants/CNGC2 and 4. Here the response is preferentially transduced through SA-mediated pathways but is directed to JA/ethylene pathways if the SA pathway is disrupted (Genger et al., 2008). JA is made in the vasculature (xylem contact cells and phloem) and exported radially (cell-to-cell) in the leaf into different cell layers (Nguyen et al., 2017). Hence localization to the vasculature might be crucial in connecting CNGC19 with herbivory-induced jasmonates. We identified that CNGC19 interacts strongly with herbivory-activated CaM2 in planta. Recently, a mechanistic link between Ca^{2+} and jasmonate biosynthesis has been shown via the JAV1–JAZ8–WRKY51 complex that represses expression of JA biosynthesis genes in healthy plants. Upon wounding, CaM1, CaM4, and CaM7 sense Ca^{2+} elevation and interact with JAV1, which results in its phosphorylation, and subsequent de-repression of JA biosynthesis and rapid burst of JA for plant defense (Yan et al., 2018). It is possible that CNGC19 with a C-terminal CaM binding site could be upstream to this process, and loss-of-function affects the JA burst upon herbivory; however, this hypothesis warrants further study.

CNGC19 Modulates Aliphatic GS Biosynthesis via Regulating *BCAT4* Expression

GSs act as a feeding deterrent against generalist herbivores via their toxic breakdown products (isothiocyanates, nitriles, and epithionitriles; Textor and Gershenzon, 2009). Aliphatic and indole

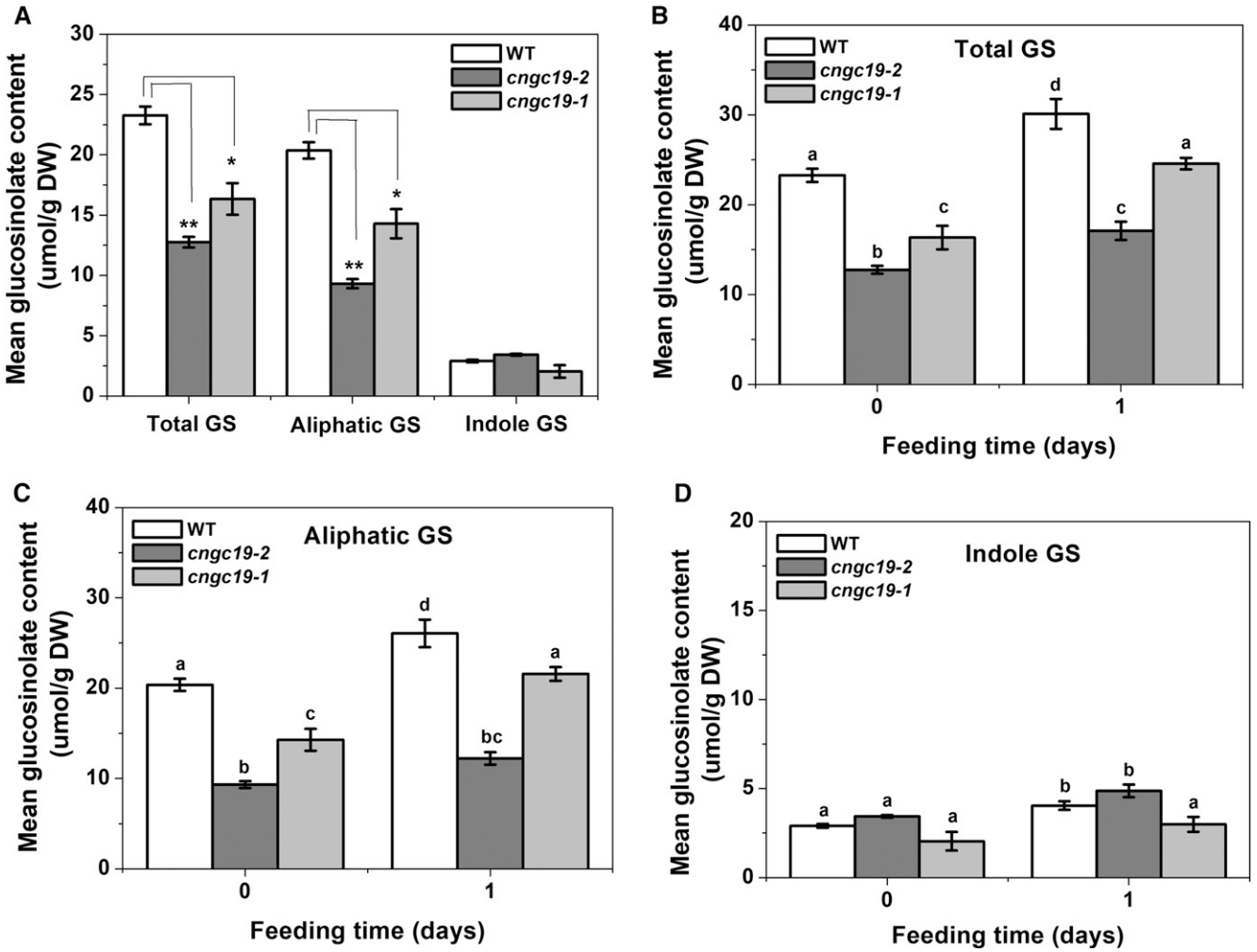

Figure 6. GS Levels Are Modulated in *cngc19* Mutants.

(A) Mean ± SE ($n = 8$) Total, aliphatic, and indole GS levels in rosette leaves of 5-week–old untreated Arabidopsis wild-type (white bars), *cngc19-2* (dark gray bars), and *cngc19-1* (light gray bars) plants. Statistically significant differences between plants were analyzed by unpaired *t* test: $*P \leq 0.05$; $**P \leq 0.001$. DW, dry weight; WT, wild type.

(B) to **(D)** Total, aliphatic, and indole GSs levels in rosette leaves of 5-week–old Arabidopsis wild-type (white), *cngc19-2* (dark gray), and *cngc19-1* (light gray) plants fed on by Spodoptera larvae (fourth-instar) for 1 d. Statistically significant differences among treatments were analyzed by one-way ANOVA with a posthoc SNK test ($P \leq 0.05$). Values are means of two independent experiments ($n = 8$). Two-way ANOVA combining the two *cngc19* alleles is depicted in Supplemental Table 3. DW, dry weight; WT, wild type.

GS have an additive negative effect on *Spodoptera exigua* growth (Müller et al., 2010). The *cngc19* lines constitutively and upon herbivory have reduced aliphatic GS content compared with wild type. Reduced aliphatic GS correlates with an increase in its precursor, Met, suggesting that *cngc19* is defective in conversion of Met to aliphatic GS. Branched-chain aminotransferases BCAT4, BCAT3, and BCAT6 are involved in the biosynthesis of aliphatic GS. Among them, *BCAT4* is the major gene that catalyzes the first part of the biosynthesis of Met-derived aliphatic GSs, which is the transamination of Met to 4-methylthio-2-oxobutanoate (Schuster et al., 2006; Lächler et al., 2015). Expression of the branched-chain aminotransferase *BCAT4* is greatly reduced in both *cngc19* mutants. *BCAT3* and *BCAT6* transcript levels are unaltered in *cngc19*, and this could account for the slight increase in aliphatic GS content in *cngc19* upon *S. litura* herbivory. *cngc19* also showed downregulation of *BCAT1* and *BCAT2*, which are not involved in aliphatic GS biosynthesis (Angelovici et al., 2013). In Arabidopsis, GTR1 and GTR2 are involved in bi-directional long-distance transport of aliphatic GSs from shoot to root (Andersen et al., 2013). The minor downregulation of *GTR1* and *GTR2* expression in *cngc19* rosettes might be a secondary effect of reduced biosynthesis of aliphatic GS and hence reduced transport. The excess of Met in *cngc19* leads to an increase of its transport compound, SMM. Plant SMM transporters are not known, but expression of a yeast SMM transporter in pea resulted in improved sulfur and nitrogen content of the seeds (Tan et al.,

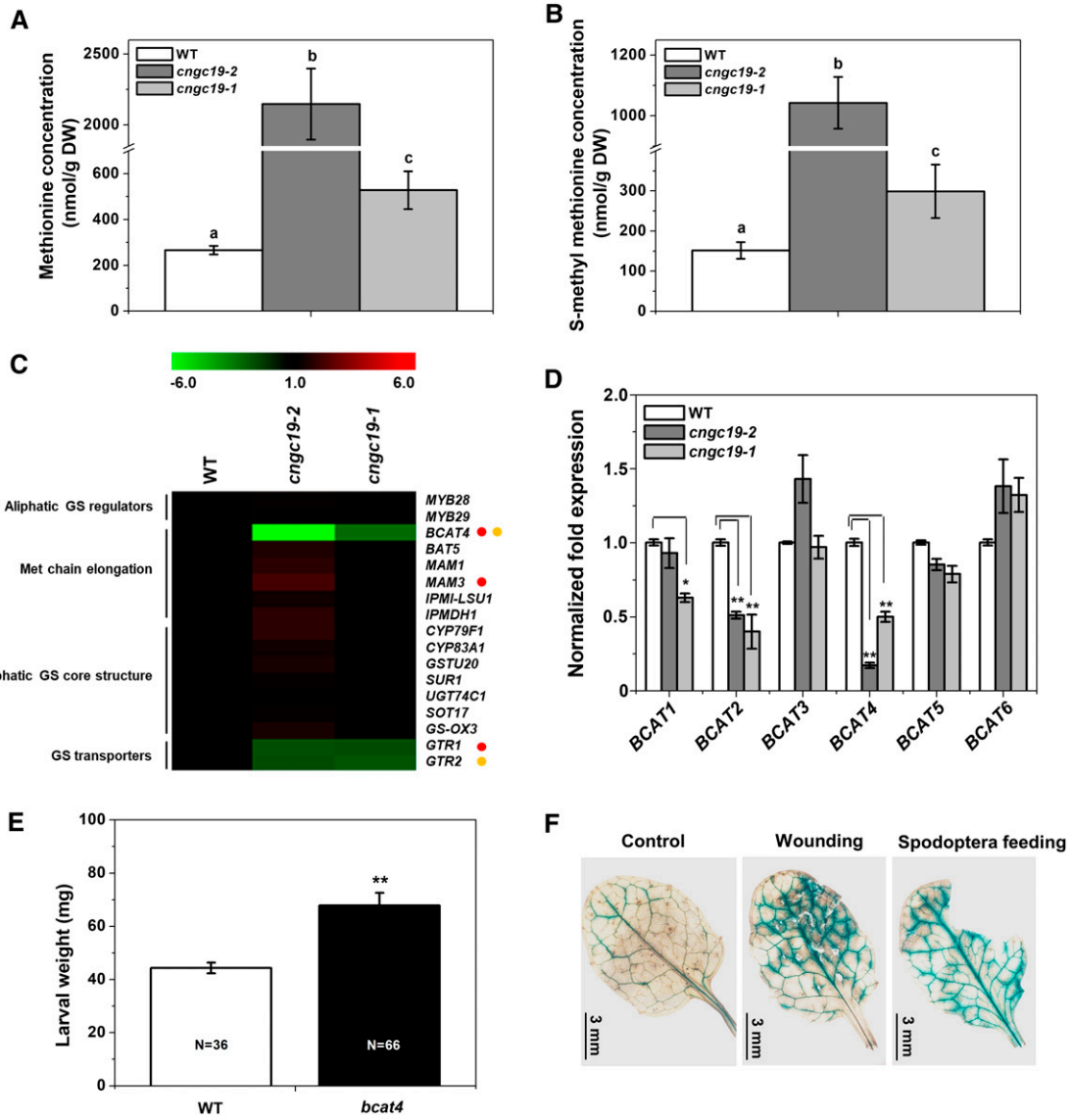

Figure 7. SMM Contents in *cngc19* Mutants.

(A) and **(B)** SMM levels in rosette leaves of 5-week-old Arabidopsis wild-type (white), *cngc19-2* (dark gray), and *cngc19-1* (light gray) plants in control conditions. Statistically significant differences among genotypes were analyzed by one-way ANOVA with a posthoc SNK test ($P \leq 0.05$). Values are means of two independent experiments ($n = 8$). WT, wild type.

(C) Heat map represents expression of aliphatic GS pathway genes analyzed in 6-week–old wild type and *cngc19* mutants leaves. Gene transcript abundance was determined by real-time PCR, and samples were normalized by plant *RPS18* mRNA. Fold change is the mean ± SE ($n = 4$). Statistically significant differences between plants were analyzed by unpaired *t* test: $P \leq 0.05$. Red and yellow circles represent statistically significant differences between wild type with *cngc19-2* and *cngc19-1*, respectively. WT, wild type.

(D) Normalized fold expression of all six members of *BCAT* gene family analyzed in 6-week–old wild-type and *cngc19* mutants' leaves. Gene transcript abundance was determined by real-time PCR, and samples were normalized by plant *RPS18* mRNA. Fold change is the mean ± SE ($n = 4$). Statistically significant differences between Col-0 and *cngc19* mutant lines were analyzed by unpaired *t* test: $^{*}P \leq 0.05$; $^{**}P \leq 0.001$. WT, wild type.

(E) Mean (mean ± SE) larval weight after feeding on wild-type (Col-0) and *bcat4* mutant. The larval weight was measured after 8 d of feeding. The total number of larvae weighed (*N*) is indicated in the bars. Statistically significant difference between wild-type and *bcat4* was analyzed by one-way ANOVA with a posthoc SNK test ($^{**}P \leq 0.001$). WT, wild type.

(F) *BCAT4* promoter early activated upon 5 min of mechanical wounding and Spodoptera herbivory. After treatments, leaf tissues were collected from the *ProBCAT4*:*GUS*-expressing transgenic line and incubated in GUS staining solution for 1 h.

A

GO-ID	Biological process	p-value	% Gene enrichment
50896	Response to stimulus	3.36E-03	18.65
44403	Symbiosis, encompassing mutualism through parasitism	6.12E-03	0.55
9695	Jasmonic acid biosynthetic process	1.16E-02	0.55
6810	Transport	1.23E-02	9.32
9607	Response to biotic stimulus	1.43E-02	4.10
9416	Response to light stimulus	1.46E-02	3.54
9611	Response to wounding	1.52E-02	1.49
9694	Jasmonic acid metabolic process	1.71E-02	0.55
55074	Calcium ion homeostasis	2.38E-02	0.55
42221	Response to chemical stimulus	2.40E-02	10.07
9816	Defense response to bacterium, incompatible interaction	2.63E-02	0.55
9870	Defense response signaling pathway, R gene-dependent	2.75E-02	0.37
9914	Hormone transport	3.39E-02	0.74

B

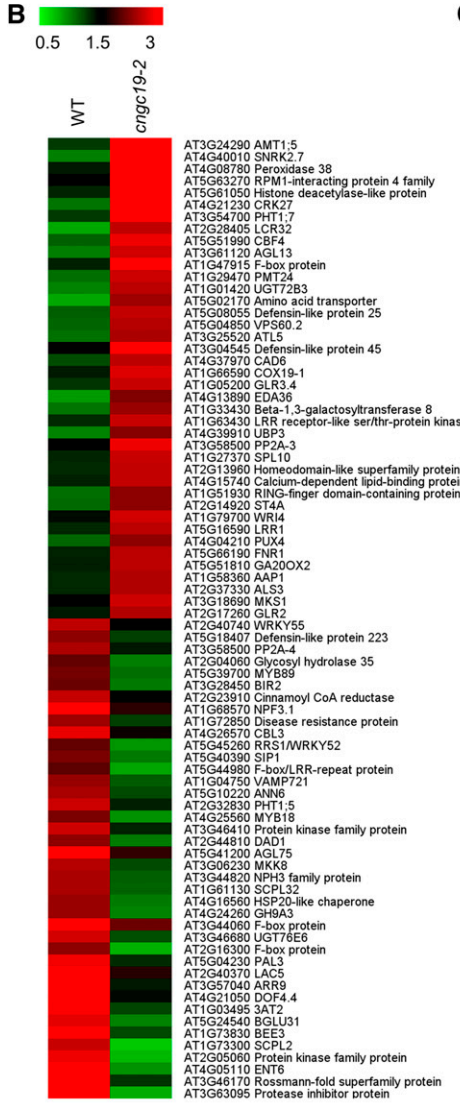

C

Gene id	Gene name	Transcript name	Fold change	*p*-value
		Transporters		
AT3G24290	AMT1;5	Ammonium transporter 1;5	4.58	0.041658
AT3G54700	PHT1;7	Phosphate transporter 1;7	3.28	0.001937
AT5G02170		Amino acid transporter family protein	2.76	0.015565
AT1G58360	AAP1	Amino acid permease 1	2.14	0.046868
AT5G53510	OPT9	Oligopeptide transporter 9	2.09	0.026506
AT5G25430		Boron transporter 6	1.91	0.016484
AT5G09930	GCN2	ABC transporter F family member 2	1.85	0.005777
AT1G52190	NRT1.11	nitrate transporter 1.11	1.65	0.023181
AT1G05580	CHX23	Cation/H(+) antiporter 23	1.63	0.009492
AT5G22830	MGT10	Magnesium transporter 10	1.63	0.035428
AT2G32830	PHT1;5	Phosphate transporter 1;5	-2.31	0.00901
AT1G68570		putative nitrite transporter	-2.1	0.024648
AT5G57685	GDU3	Glutamine dumper 3	-1.92	0.044936
AT1G49810	NHD2	Na+/H+ antiporter 2	-1.9	0.049293
AT3G28360	PGP16	ABC transporter B family member 16	-1.85	0.009977
AT3G03090	VGT1	Vacuolar glucose transporter 1	-1.84	0.011492
		JA biosynthesis and signaling		
AT1G17380	JAZ5	protein TIFY 11A	1.85	0.047859
AT1G72520	LOX4	Lipoxygenase 4	1.71	0.001422
AT1G17420	LOX3	Lipoxygenase 3	1.69	0.011847
AT2G44810	DAD1	phospholipase A(1) DAD1	-2.33	0.048953
AT1G55020	LOX1	Lipoxygenase 1	-1.5	0.024842
		Hormone Signaling		
AT4G40010	SNRK2.7	SNF1-related protein kinase 2.7	4.46	0.011688
AT3G58500	PP2A-3	Ser/thr-protein phosphatase PP2A-3 catalytic subunit	2.31	0.032034
AT5G51810	GA20OX2	Gibberellin 20 oxidase 2	2.16	0.00294
AT3G56380	ARR17	Two-component response regulator ARR17	1.97	0.041863
AT4G28140	ERF054	Ethylene-responsive transcription factor ERF054	1.64	0.015044
AT3G26090	RGS1	Membrane receptor protein RGS1	1.55	0.011952
AT3G57040	ARR9	two-component response regulator ARR9	-2.85	0.043026
AT3G58500	PP2A-4	Ser/thr-protein phosphatase PP2A-3 catalytic subunit	-2.02	0.011014
AT5G13330	Rap2.6L	Ethylene-responsive transcription factor ERF113	-1.97	0.016491
AT4G00710	BSK3	BR-signaling kinase 3	-1.89	0.036129
AT1G75450	CKX5	Cytokinin dehydrogenase 5	-1.66	0.031494
AT1G10470	ARR4	Two-component response regulator ARR4	-1.62	0.041911
AT3G48100	ARR5	two-component response regulator ARR5	-1.61	0.012838
AT4G36110		SAUR-like auxin-responsive protein	-1.56	0.030136
AT3G29575	AFP3	Ninja-family protein AFP3	-1.56	0.020294
		LRR proteins		
AT4G21230	CRK27	Cysteine-rich receptor-like protein kinase 27	3.48	0.017901
AT3G09240	BSK9	Protein kinase protein with tetratricopeptide repeat domain	3.44	0.036117
AT1G63430		LRR receptor-like serine/threonine-protein kinase	2.35	0.01707
AT5G16590	LRR1	Leucine-rich repeat protein 1	2.21	0.017629
AT2G27060		Leucine-rich repeat protein kinase-like protein	1.9	0.033503
AT3G28450		Leucine-rich repeat protein kinase-like protein	-2.08	0.048974
AT3G50690		Leucine-rich repeat (LRR) family protein	-1.88	0.040058
AT5G38990		Receptor-like protein kinase	-1.87	0.021324
AT5G16900		LRR receptor-like serine/threonine-protein kinase	-1.68	0.007418
AT5G18500		Receptor-like protein kinase	-1.66	0.010995
AT5G13290	CRN	Leucine-rich repeat receptor-like protein kinase CORYNE	-1.64	0.031543
AT1G72460		Leucine-rich repeat transmembrane protein kinase	-1.58	0.006864
AT1G70530	CRK3	Cysteine-rich receptor-like protein kinase 3	-1.57	0.005667
		Defense related proteins		
AT5G63270		RPM1-interacting protein 4 family protein	3.65	0.009514
AT5G08055		Defensin-like protein 25	2.61	0.03482
AT3G04545		Defensin-like protein 45	2.46	0.040538
AT1G05200	GLR3.4	Glutamate receptor 3.4	2.41	0.032943
AT2G17260	GLR2	Glutamate receptor	2.06	0.000968
AT4G08500	MEKK1	mitogen-activated protein kinase kinase kinase 1	1.96	0.007652
AT1G19320		Pathogenesis-related thaumatin-like protein	1.94	0.035832
AT5G41740		TIR-NBS-LRR class disease resistance protein	1.88	0.031567
AT5G18370		TIR-NBS-LRR class disease resistance protein	1.87	0.041027
AT1G12663		Pathogenesis-related protein	1.74	0.018089
AT1G28335	LCR31	low-molecular-weight cysteine-rich 31	1.6	0.024827
AT2G46070	MPK12	mitogen-activated protein kinase 12	1.54	0.039559
AT3G06230	MKK8	MAP kinase kinase 8	-2.37	0.005608
AT5G45260	RRS1	Disease resistance protein RRS1	-2.16	0.005971
AT1G72850		TIR-NBS class of disease resistance protein	-2.1	0.049724
AT5G18407		Defensin-like protein 223	-2.01	0.021307
AT2G40740	WRKY55	WRKY transcription factor 55	-2	0.004741
AT2G03933		Defensin-like protein 59	-1.89	0.027104
AT4G04700	CPK27	calcium-dependent protein kinase 27	-1.67	0.015817
AT5G05680	MOS7	MODIFIER OF SNC1,7	-1.62	0.021771
AT2G32390	GLR3.5	Glutamate receptor 3.5	-1.76	0.002104

Figure 8. Global Expression Profiling of Genes in *cngc19-2* and Wild Type after 24 h of Spodoptera Herbivory.

(A) Highly enriched GO terms for the differentially expressed transcripts after Spodoptera herbivory for 24 h in *cngc19-2* mutant plants. All the differentially expressed transcripts (>1.5 fold) were subjected to GO enrichment analysis. Important biological processes with *P* value and % gene enrichment are shown. For the enrichment, the *P*-value cutoff was < 0.05.

(B) Heat map depicting the expression profile of the 80 highest up- or downregulated genes in microarray comparing the *cngc19-2* mutant with wild type after 24 h of Spodoptera herbivory (fourth-instar larvae). Color scale represents average intensity values in $\log_2$. WT, wild type.

(C) List of selected genes altered in microarray. Fold change is calculated by *cngc19-2*+Spodoptera/wild-type+Spodoptera.

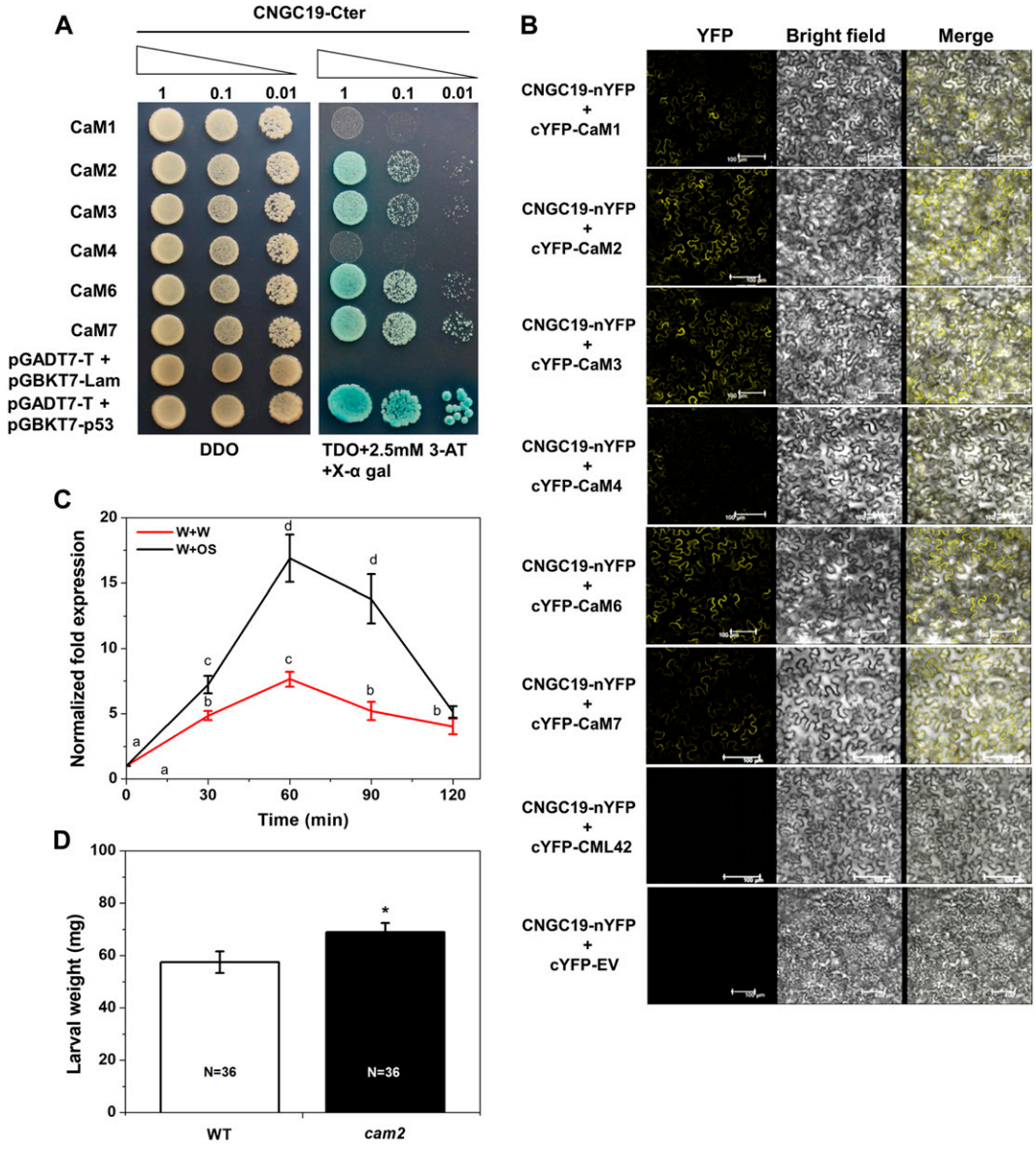

Figure 9. CNGC19 Interacts with Herbivory-Induced CaM2 In Planta.

(A) Y2H interaction study of CNGC19 and CaMs. Y2H gold yeast cells cotransformed with pGBKT7-CNGC19 C-terminal and pGADT7-CaM1, CaM2, CaM3, CaM4, CaM6, and CaM7 were grown in nonselective SD-*Leu*/-*Trp* (DDO) medium to $OD_{600} = 1$. Ten μL from a 10-time dilution series were spotted on control nonselective DDO and selective TDO medium containing 2.5-mM 3-AT and X-α gal. Diminution of cell density in the dilution series is indicated by narrowing triangles. SV40 large T-antigen and p53 interaction was used as a positive control whereas T-antigen with lamin (Lam) DNA served as a negative control.
(B) Protein–protein interactions between CNGC19 and CaMs. A BiFC assay was performed using CNGC19 fused with the N-terminal part of YFP and CaMs (CaM1, 2, 3, 4, 6, and 7) fused with the C-terminal part of YFP and transiently expressed in *N. benthamiana* by Agrobacterium-mediated infiltration. Images show YFP-mediated fluorescence derived from the protein–protein interaction; the brightfield image shows the plasma membrane and the superimposed images are of brightfield and YFP (Merge). Scale bar = 100 μm. Interaction of CNGC19 with CML42 is shown as a negative control, as these proteins do not interact even in Y2H.
(C) *CaM2* transcript levels in Arabidopsis leaves treated with *Spodoptera* OS for 30, 60, 90, and 120 min. Leaves were wounded with a pattern wheel and subsequently 20 μL of water or 1:1 diluted OS per leaf was applied. Gene transcript abundance was determined by real-time PCR and samples were normalized by plant *RPS18* mRNA. The graphs show fold change of mRNA level relative to the untreated control. Fold change is the mean ± SE ($n = 4$).
(D) Mean (mean ± SE) larval weight after feeding on the wild-type (Col-0) and *cam2* (SALK_114166C) mutant. The larval weight was measured after 8 d of feeding. The total number of larvae weighed (*N*) is indicated in the bars. Statistically significant differences between wild type and *cam2* after a feeding assay were analyzed by one-way ANOVA with a posthoc SNK test (*$P \leq 0.05$).

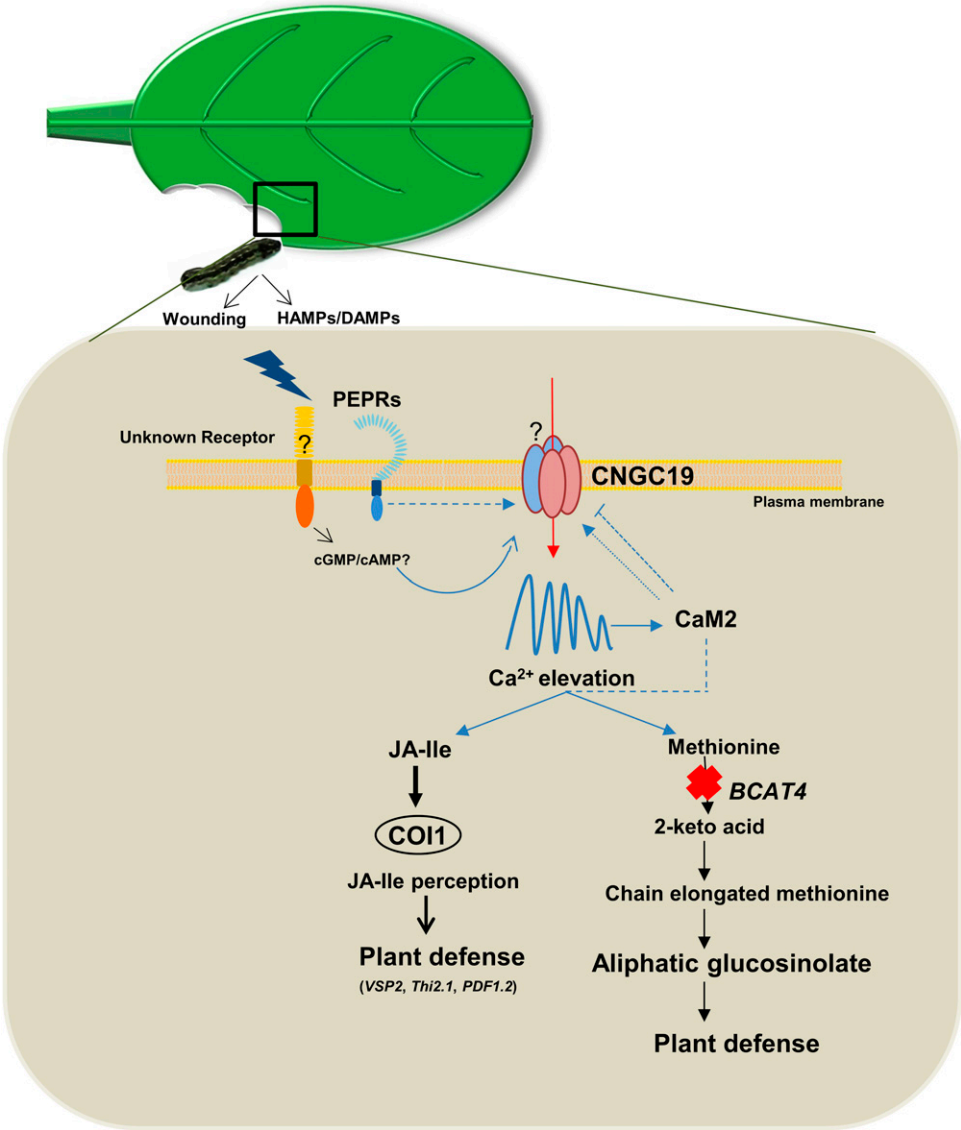

Figure 10. Model for a Role of Arabidopsis CNGC19 in Plant Defense against *S. litura* Herbivory.

Upon *S. litura* herbivory, unknown receptors and PEPR perceive wounding and HAMPs/DAMPs, and activate a plasma-membrane–localized, CNGC19. This generates cytosolic Ca^{2+} elevation, which activates downstream defense signaling. *CNGC19* is expressed in leaf vasculature and is crucial for wound-induced intravascular Ca^{2+} fluxes within a leaf. CNGC19 positively regulates Arabidopsis defense, as loss-of-function of *CNGC19* results in increased *S. litura* herbivory and breakdown of plant defense. CNGC19 interacts with the Ca^{2+}-sensor CaM2 in planta and this might regulate the channel and contribute to plant defense. Loss-of-function of *CNGC19* also results in alteration in the Pep-induced Ca^{2+} signature. CNGC19 acts as positive regulator of plant defense by the action on JA-Ile biosynthesis and its expression depends on the JA receptor COI. Loss-of-function of *CNGC19* results in the downregulation of aliphatic GS levels and hyperaccumulation of their precursor, Met. CNGC19 modulates aliphatic GS biosynthesis by regulating *BCAT4* expression. Arrows imply activation in all cases and broken lines indicate a possible role in a process. T-bars indicate inhibition of a process.

2010) and consistent with these data, we see the expression of many nutrient uptake genes and amino acid transporters (AMT1, AAP) in our microarray with *cngc19* and wild type, indicating that excess Met is rerouted for nutrient mobilization. In leaves, constitutive BCAT4 promoter activity was found in veins (Schuster et al., 2006). We found that upon Spodoptera feeding *BCAT4* is also exclusively expressed in vasculature. Interestingly, both *BCAT4* and *CNGC19* are phloem-expressed and wound-inducible genes (Schuster et al., 2006; Kugler et al., 2009). How CNGC19 regulates cytosolic BCAT4 is unknown. GSs are more abundant in the midvein and the periphery of the leaf than the inner lamina. So, some chewing insects avoid the midvein and leaf periphery when feeding on Arabidopsis leaves (Shroff et al., 2008). Hence, vasculature localization of BCAT4 and CNGC19 might be important for their coregulation and to influence GS biosynthesis. They might also be part of protein complexes in native uninduced stages that regulate

each other's expression. Other Ca^{2+}-regulated genes known to influence GS biosynthesis are Ca^{2+}/CaM-related IQ-DOMAIN1 (Levy et al., 2005), CML42 (Vadassery et al., 2012), and CALMODULIN BINDING TRANSCRIPTION ACTIVATOR3 (Laluk et al., 2012). None of these are in the biosynthetic pathway for GS. From multiple reports and our work, it is clear that GS biosynthesis is intricately linked to Ca^{2+} signaling. CNGC channels and interacting CaMs might be key regulatory players.

Plant CNGCs are both positively and negatively regulated by the Ca^{2+} sensor CaM by apoCaM binding to an isoleucine glutamine motif in the C terminus of CNGCs and/or Ca^{2+}/CaM binding both N- and C-terminal motifs with different affinities (Fischer et al., 2013; DeFalco et al., 2016). We show that CNGC19 interacts with herbivory-specific CaM2 in planta. We found that CaM2 is a positive regulator of herbivore defense and insects feed more on *cam2* mutants than on wild-type plants. From the literature it is known that CaM2 (TCH1) is upregulated by both touch and darkness (Lee et al., 2005; McCormack et al., 2005). In vegetative organs, the *CaM2* gene was specifically expressed in the vascular tissue and involved in pollen germination (Landoni et al., 2010). The Ca^{2+} sensor CaM2 can act to both regulate CNGC19 channel activity and downstream plant defense (e.g. jasmonate biosynthesis). CaM2 could be a potential target for generating double mutants with CNGC19, to elucidate its role in plant defense to herbivores.

Our data demonstrate that CNGC19 is crucial in the perception of herbivory by regulating the Ca^{2+} fluxes and coupling it to downstream defense signaling (Figure 10). The vasculature seems to be an important hub for plant defense against herbivory where CNGC19 and all associated proteins reported in the study (CaM2, BCAT4, PEPRs, jasmonate, and GS biosynthesis) are localized (Figure 10). The mechanisms by which plants couple CNGC19 channel activation to induced defenses vis-à-vis JA-Ile and aliphatic GS biosynthesis, form an interesting area for future research. Future biochemical studies on single and multiple CNGC mutants will be necessary to elucidate their role in the generation of both local and systemic Ca^{2+} elevation upon *S. litura* herbivory. Subunit composition affects the functional properties of a channel, and it is possible that a combinatorial code of channel tetrameric composition determines the specificity of stress perception. Identification of protein complexes of CNGC19 with other CNGCs, and other putative subunits expressed in the vasculature, would be an exciting area of research.

METHODS

Plant and Insect Materials

Arabidopsis (*Arabidopsis thaliana*) seeds (ecotype Columbia; Col-0) and mutant lines with a T-DNA insertion in the exon of *AtCNGC19* (At3g17690), namely SALK_129200C and SALK_027306 (provided by TAIR; Alonso et al., 2003) were used. The absence of *CNGC19* mRNA in the homozygous SALK_ 129200C and SALK_27306 were checked by RT-PCR using *CNGC19* gene-specific primers. The *cngc19-1* (SALK_27306) line has been characterized for its involvement in salt stress in Kugler et al. (2009). *AtCNGC20* (SALK_0129133C) and *AtCaM2* (SALK_114166C) were also obtained from TAIR. The *cam2* line was previously characterized by Zhang et al. (2009). The *bcat4* (AT3G19710) mutant line SALK_013627 was kindly provided by Stefan Binder (University of Ulm). *pepr1 pepr2* double mutants were provided by Gerald Berkowitz (University of Connecticut). GCaMP3 lines were gifted by Dale Sanders (John Innes Centre). Seeds were sown in 10-cm pots and stratified for 2 d at 4°C in darkness. Afterwards, plants were moved to ventilated growth rooms with constant air flow and 60% humidity at 22°C. Plants were grown at a 10-h light/14-h dark photoperiod and a light intensity of 150 μmol m^{-2} s^{-1}. Larvae of *Spodoptera litura* were hatched from eggs and reared on an agar-based optimal diet (Bergomaz and Boppré, 1986). The insect biomass assay was done using first-instar larvae (freshly hatched larvae grown for 3 d in light), which were preweighed before the experiment and selected to have equal weights. Three larvae were placed on a single plant and covered with perforated plastic covers. After 8 d of feeding, all larvae were removed and weighed individually. Each experiment had 10 plants and the experiments were repeated three to four times independently. For phytohormone and GS estimation, 1-d feeding was performed with fourth-instar *S. litura* larvae which were starved 12 h before plant feeding.

Plant Treatments

All simulated herbivory experiments were performed 6 weeks post-germination at a vegetative (prebolting) growth stage. For experiments with insect OSs, the adaxial (upper) side of the leaf was wounded with a pattern wheel (six vertical motions). Fourth-instar *S. litura* larvae were reared on an artificial diet of Arabidopsis leaves for 24 h before collecting OS on ice. The OS was centrifuged at 13,000 rpm for 2 min and diluted 1:1 with water. A total of 20 μL of fresh diluted OS was spread across all the holes on a single leaf (W + OS). In control plants, water was added (W+Water). *coi1-1* homozygous plants were selected by CAPS marker (Xie et al., 1998). This method for simulated herbivory was also used for *CNGC19* expression in the *coi1-1* and *pepr1 pepr2* mutant lines. For *CNGC19* expression analysis in systemic leaves upon simulated herbivory, leaves were numbered, leaf number 8 was wounded with a pattern wheel, and water/OS was applied. Systemic leaves 5, 11, 13, and 16 are known to have vascular connection with leaf number 8 (Mousavi et al., 2013; Kiep et al., 2015), and were harvested after 30 min and 60 min for gene expression studies. For *CNGC19* expression in Spodoptera-fed plants, fourth-instar *S. litura* larvae were transferred to wild-type plants and allowed to feed for the indicated time intervals. Chemically synthesized JA-Ile (Walter et al., 2007; Scholz et al., 2014) was dissolved in 100% ethanol to make 300-mM stock, which was then diluted in water to a final concentration of 500 μM. Fourteen-d–old seedlings were treated with 500-μM JA-Ile for the indicated time intervals.

CNGC19 and *BCAT4* Promoter Reporter Assays

For the promoter β-glucuronidase (GUS) fusion construct, a 2.6-kb fragment upstream of the translation start codon of *CNGC19* including the first exon was amplified ($\sim$3-kb fragment) from genomic DNA and was cloned in the pBI101.2 vector at the *Sal*I/*Bam*HI sites. An $\sim$2.2-kb genomic fragment upstream of the translation start codon of *BCAT4* was amplified and cloned in the pBI101.2 vector at the *Sal*I/*Bam*HI sites for the BCAT4 promoter-GUS fusion construct. For GUS reporter staining, Arabidopsis leaves from *ProCNGC19*:*GUS*- and *ProBCAT4*:*GUS*-expressing transgenic plants (T_3 generation) were vacuum-infiltrated with GUS staining solution (50 mM of sodium phosphate buffer at pH 7.0, 2 mM of EDTA (w/v), 0.12% Triton, 0.4 mM of ferrocyanide, 0.4 mM of ferricyanide, and 1.0 mM of 5-bromo-4-chloro-3-indolyl-β-D-glucuronide cyclohexylammonium salt) for 5–15 min and incubated in the dark at 37°C for 1 h. Tissues were cleared of chlorophyll by treatment with 70% ethanol at 65°C for 1 h and analyzed by light microscopy. *ProCNGC19*:*GUS* and *ProBCAT4*:*GUS* expressing transgenic plants were wounded by needle or fed by Spodoptera (fourth-instar larvae). After 5 min of treatments leaf tissues were collected and incubated in GUS staining solution for 1 h. List of primer pairs used in this study are in Supplemental Table 1

Ca^{2+} Measurements

GCaMP3 reporters: Transgenic Arabidopsis (Col) expressing GCaMP3, and a *cngc19-2* mutant crossed with GCaMP3 (T_2), selected to ensure equal background fluorescence, were used for Ca^{2+} measurements. Four-week–old plants under short-day conditions on soil were used for the experiments. Both wild-type and *cngc19-2* GCaMP3-expressing leaf discs were also tested for their similar response to 2-M $CaCl_2$ with 20% ethanol after each experiment to ensure equal basal fluorescence (Supplemental Figure 5B). This ensured that the differences in background intensity of GCaMP3 do not account for varying signal intensity/spread in different plants. We only used local leaf (leaf 5) for wounding and imaging in all experiments. A stereomicroscope (Nikon) was used to visualize the fluorescence, with GFP excitation at 470 nm and emission at 500 to 550 nm. Basal fluorescence level of unwounded leaf was captured by a camera (Nikon) with 4× gain and 5-s exposure time. In leaf 5 of wild type and *cngc19*, leaf lamella including midrib was wounded using sharp scissors and fluorescence was captured at every 5-s interval for 5 min. Mean fluorescence of images were calculated using the software ImageJ 1.52a (U.S. National Institutes of Health). TIFF files were used for data processing and whole-leaf mean fluorescence, excluding the cut region, was calculated by selecting the leaf area using a freehand selection tool (Supplemental Figure 5). Normalized fluorescence intensity ($\Delta F/F$) was calculated according to $\Delta F/F = F - F_0/F_0$ (F, fluorescence after wounding; F_0, basal fluorescence intensity) and was performed as described in Toyota et al. (2018). Spodoptera feeding and visualization of signals in the same leaf is technically challenging and was not done, unlike in Toyota et al. (2018), where systemic signals upon feeding were probed.

Aequorin (Aeq) reporters: Transgenic Arabidopsis (Col-0)-expressing cytosolic apoaequorin (Knight et al., 1997) and *cngc19-2* mutant seedlings transformed with pMAQ2 vector (T_2) with good discharge were used for Ca^{2+} measurements. Aeq and *cngc19*-pMAQ2 seedlings were grown in liquid MS medium and 12-d–old seedlings were transferred into a 96-well white plate (Thermo Fisher Scientific) containing 5-μM coelenterazine (PJK International) in the dark overnight at 21°C. Bioluminescence counts in seedlings were recorded as relative light units per s with a microplate luminometer (Luminoskan Ascent, v2.6; Thermo Fisher Scientific). After 102-s background reading, 20-nM Pep1 (GenScript) was added manually to the well and readings in relative light units per s were taken for 900-s Calibrations were performed by estimating the amount of Aeq remaining at the end of experiment by discharging all remaining Aeq with 2 M of $CaCl_2$ with 20% ethanol, and the counts were recorded for 360 s. The luminescence counts obtained were calibrated using the equation from Rentel and Knight (2004).

cAMP Quantification

For cAMP quantification, leaves of 6-week–old wild-type plants and *pepr1 pepr2* mutants were treated with *S. litura* OS for 2.5 and 5 min. Samples were ground in liquid N_2 to form fine powder and cAMP was extracted by homogenizing in 500-μL lysis buffer (50 mM of Tris-HCl at pH 7.5, 100 mM of NaCl, 0.1% Triton, 1 mM of DTT, 2 mM of EDTA, and protease inhibitor cocktail [Roche]). After 30 min of incubation on ice, samples were centrifuged at 13,000 rpm for 5 min at 4°C. Supernatant was collected and protein amount was quantified. cAMP was measured according to the user manual provided with the cAMP ELISA Kit (Cayman Chemical).

TEVC in *Xenopus* Oocytes

The CNGC19-YFP fragment was amplified from the pEG101-CNGC19:YFP construct and subcloned into vector pGEMHE in *Bam*HI/*Eco*RI restriction sites (Liu and Luan, 2001). Oocytes were isolated by mini-laparotomy from adult female *Xenopus laevis*. Surgical procedures for oocyte collection were approved by the Institutional Animal Ethics Committee, which reports to the Committee for the Purpose of Control and Supervision of Experiments on Animals, Government of India. Clusters of oocytes were broken down with collagenase and individual oocytes defolliculated manually. Oocytes at stages V to VI were selected and incubated in ND-96 solution (96 mM of NaCl, 2 mM of KCl, 1 mM of $MgCl_2$, 1.8 of mM $CaCl_2$, and 5 mM of HEPES at pH 7.5, supplemented with 2.5 mM of sodium pyruvate and enriched with Horse serum) with 50-μg/mL penicillin/streptomycin at 18°C overnight before injections. Capped RNA was prepared from the linearized plasmid DNA templates using the Ampli-Cap Max T7 Message Maker kit (CellScript), following the manufacturer's instructions. Approximately 10 ng of each cRNA was injected into each oocyte. Electrophysiological experiments were performed 48 to 96 h after injection using a TEC-10CX TEVC Amplifier (NPI Electronic) to maintain holding potentials and record membrane currents. The analog output of the amplifier was sampled at 10 kHz and filtered at 3 kHz, digitized, and stored for further analysis. The software package pCLAMP v10.2 (Molecular Devices) was used to generate voltage clamp commands, acquire membrane currents, and analyze digitized data. All experiments were performed at room temperature. All experimental data were first analyzed with Clampfit v10.2 (pCLAMP; Molecular Devices) and exported to the software Origin v8.0 (OriginLabs) for subsequent analysis and display. The bath solution was 200-mM–mannitol buffered with MES-Tris to pH 7.4. Additions made were: 300 μm of dibutyryl cAMP with a 15-min incubation period, followed by $CaCl_2$ (15 mM), and finally DIDS (300 μM). NaCl (10 mM) and KCl (10 mM) were added before CaCl2 on some runs to check for the selectivity of the channel. DIDS was used to inhibit Ca^{2+}-activated Cl^- channels. Oocytes were held at −80 mV, stepped to potentials ranging from −130 mV to +40 mV, and finally brought to −60 mV. Tail currents at −60 mV were analyzed as a measure of channels open at the end of the step episode.

Confocal Microscopy to Detect Expression and Localization of CNGC19-YFP in Oocytes

Xenopus oocytes injected with either water or CNGC19-YFP and were imaged in bright field and in fluorescence confocal mode. Oocytes were imaged with a 10× Plan Apochromat objective on a LSM-780 Confocal Microscope (Zeiss) 36 to 48 h postinjection. YFP was excited using the 514-nm line of a multi-line Argon laser while the emission was recorded using a spectral detector over 523 to 675 nm. Line scans were performed on fluorescence images of both CNGC19-YFP and water-injected oocytes.

Vector Construction and Expression of YFP Fusion Protein

Gateway Technology (Invitrogen) was used for the generation of pEG101 transformation constructs, which consisted of a target gene (CNGC19 ORF cDNA) bearing a C-terminal fusion to YFP under the control of an enhanced Cauliflower Mosaic Virus 35S promoter for plant transformations (Earley et al., 2006). The attB adaptor-bearing PCR primers were designed for the generation of attB PCR products for recombination with the donor vector pDONR207 via BP Clonase reactions (Invitrogen). Fully sequenced entry clones were recombined in LR Clonase (Invitrogen) reactions with the pEG101 destination vector. The binary constructs were introduced into *Agrobacterium tumefaciens* (GV3101) and used for transient expression of CNGC19 in *N. benthamiana* leaves. Overnight grown cell cultures were collected and resuspended in 1 mL of infiltration buffer (10 mM of MES-KOH at pH 5.6, 10 mM of $MgCl_2$, and 150 mM of acetosyringone) to optical density at 600 nm (OD_{600}) to 0.8. The working suspensions were prepared by mixing Agrobacterium harboring *CNGC19-YFP* construct, organelle markers for plasma membrane (PM-mCherry) or tonoplast (TP-mCherry; Nelson et al., 2007), and p19 silencing suppressor in (1:1:1) ratio, incubated at room temperature for 3 h and infiltrated into the abaxial surface of fully developed leaves. Plants were cultivated for 3 d under growth-room

conditions (28°C temperature, 16-h light/8-h dark photoperiod with one bulb of cool white and five bulbs of wide spectrum lights with a light intensity of 150 μmol m^{-2} s^{-1}) and the infiltrated leaf area was analyzed by confocal laser scanning microscopy using a TCS SP5 (Leica Microsystems) equipped with appropriate lasers (514 to 527 nm and 587 to 610 nm for YFP and mCherry, respectively). Autofluorescence of chloroplasts was detected at 650 to 700 nm. For stable line preparation, Arabidopsis flowering plants were transformed by floral dip method, as described in Clough and Bent (1998).

Protein Extraction and Immunoblot

Microsomes were prepared from CNGC19-YFP transiently expressed in *N. benthamiana* leaves by homogenizing in grinding buffer (50 mM of HEPES-KOH at pH 7.5, 10 mM of EDTA, 330 mM of Suc, 0.6% polyvinylpolypyrrolidone, 1 mM of DTT, 1 mM of PMSF, and 1% protease inhibitor cocktail). The extract was centrifuged at 18,000*g* for 10 min and the supernatant was further centrifuged at 100,000*g* for 1 h. The microsome pellet was then resuspended in resuspension buffer (20 mM of HEPES-KOH at pH 7.5, 1 mM of EDTA, 330 mM of Suc, 1 mM of PMSF, and 1% protease inhibitor cocktail). Crude microsome fraction was separated by SDS-PAGE and transferred onto a nitrocellulose membrane. The membrane was incubated first with rabbit anti-GFP antibody (AS15 2987; Agrisera Antibodies) and then with goat-anti rabbit IgG-HRP conjugates (Merck) followed by chemiluminescence with Clarity Western ECL substrate (Bio-Rad).

Expression Analysis by Real-Time PCR

Leaf material was ground to a fine powder in liquid N_2, and total RNA was isolated using TRIzol Reagent (Invitrogen) according to the manufacturers' protocol. An additional DNase (Turbo DNase; Ambion) treatment was included to eliminate any contaminating DNA. RNA quantity was determined using Nanodrop (Thermo Fisher Scientific). DNA-free total RNA (1 μg) was converted into single-stranded cDNA using a mix of oligo-dT_{18} primers from the Omniscript cDNA Synthesis Kit (QIAGEN). Gene-specific primers (placed at the exon–exon junction for specific amplification of cDNA, whenever possible) were designed using the NCBIprimer design tool (http://www.ncbi.nlm.nih.gov/tools/primer-blast). For real-time PCR, primers producing 120- to 170-bp amplicons were used. RT-qPCR was done in optical 96-well plates on a CFX96 Real-Time PCR Detection System (Bio-Rad) using the iTaq universal SYBR green Mix (Bio-Rad). Previously optimized endogenous control *RPS18* for herbivory experiments (Vadassery et al., 2012) was used for normalization of transcripts. Fold induction values of target genes were calculated with the $\Delta\Delta^{CT}$ equation (Rao et al., 2013) and related to the mRNA level of target genes in the control leaf, which were defined as 1.0. All of the assays were run in duplicate or triplicate (biological replicates) to control for overall variability. The primer pairs used are listed in Supplemental Table 1.

Quantification of Phytohormones in Arabidopsis Leaves

Plant material was weighed (250 mg) for the wild type and *cngc19-2* mutant line and frozen with liquid N and samples were kept at −80°C until used. Wild-type and *cngc19-1* samples were lyophilized in another set of experiments and 10-mg fine powdered lyophilized tissue was used. For phytohormone analysis, finely ground leaf material was extracted with 1.5 mL of methanol containing 60 ng of d_6-JA (HPC Standards), 60 ng of salicylic acid-d_4 (Santa Cruz Biotechnology), 60 ng of abscisic acid-d_6 (Toronto Research Chemicals), and 12 ng of d_6-JA-Ile conjugate (HPC Standards) as internal standards. Phytohormones were quantified on an API 5000 LC-MS/MS system (Applied Biosystems) as described in Vadassery et al. (2012) and Scholz et al. (2017). Because it was observed that both the D6-labeled JA and D6-labeled JA-Ile contained 40% of the corresponding D5-labeled compounds, the sum of the peak areas of D5- and D6-compound was used for quantification.

GS Analysis

Whole plants were used for GS analysis as opposed to single leaves due to vast leaf to leaf variation (Brown et al., 2003). Samples were freeze-dried until constant weight and ground to a fine powder. Twenty-five mg of freeze-dried and pulverized material per plant was used for GS analysis. GS were extracted with 1 mL of 80% methanol solution containing 0.05-mM intact 4-hydroxybenzylglucosinolate as the internal standard. After centrifugation at 12,000 rpm for 10 min at 4°C, extracts were loaded onto DEAE Sephadex A-25 columns (flowthrough was collected for further metabolite analysis) and treated with arylsulfatase for desulfation (Sigma-Aldrich). The eluted desulfoglucosinolates were separated using high performance liquid chromatography (Agilent 1100 HPLC system; Agilent Technologies) on a reversed phase C-18 column (Nucleodur Sphinx RP; 250 × 4.6 mm, 5-μm particle size; Macherey-Nagel) with a water-acetonitrile gradient (1.5% acetonitrile for 1 min, 1.5% to 5% acetonitrile from 1 to 6 min, 5% to 7% acetonitrile from 6 to 8 min, 7% to 21% acetonitrile from 8 to 18 min, and 21% to 29% acetonitrile from 18 to 23 min, followed by a washing cycle; flow 1.0 mL min^{-1}). Detection was performed with a photodiode array detector and peaks were integrated at 229 nm. We used the response-factors aliphatic GS 2.0 and indole GS 0.5 (Burow et al., 2006) for quantification of individual GSs.

Amino Acid Analysis

Amino acids were analyzed in the flowthrough from the DEAE Sephadex A 25 columns used in GS analysis. Plant extracts were diluted with 1:10 (v/v) in water containing the ^{13}C-, ^{15}N-labeled algal amino acid mix (Isotec). Amino acids in the diluted extracts were directly analyzed by LC–MS/MS as described before in "Quantification of Phytohormones in Arabidopsis Leaves," with the modification that an API5000 Mass Spectrometer (Applied Biosystems) was used and the chromatographic gradient was modified as follows: 0–1 min, 3% B in A; 1–2.7 min, 3–100% B in A; 2.7–3 min 100% B, 3.1–6 min 3% B in A (A: 0.05% formic acid in water; B: acetonitrile). The mobile phase flow rate was 1.1 mL/min (Crocoll et al., 2016).

Y2H

The CNGC19 C-terminal was fused to the GAL4 DNA binding domain in pGBKT7-BD vector (Clontech Laboratories). CaM1, CaM2, CaM3, CaM4, CaM6, CaM7, and CML 42 were cloned into the pGADT7-AD vector (Clontech Laboratories) containing the GAL4 activation domain. All constructs were made using the restriction-based cloning. The pGBKT7-BD and PGADT7-AD constructs were cotransformed into the Y2H Gold strain of yeast (*Saccharomyces cerevisiae*) using a Matchmaker Gold Yeast Two-Hybrid System Kit (Clontech Laboratories), and selected for transformed cells on SD-*Leu*/-*Trp* (DDO) plates lacking Leu and Trp (−LT) and were confirmed by colony PCR. pGBKT7-T antigen was cotransformed with pGADT7-p53 or pGADT7-Lam as a positive and negative control, respectively. Y2H Gold strain cotransformed with the empty vectors, pGBKT7-BD and pGADT7-AD, was also used as a negative control. Transformed cells were grown in liquid double-dropout media (−LT) for 2 d, and adjusted to an OD_{600} of 1, 0.1, 0.01, and 10 μL. Each dilution was spotted on selection plates: DDO (−LT) and TDO (−LTH) + 2.5 mM 3-AT. For additional verification of the interaction, X α-gal, a substrate for α-galactosidase (*MEL1* reporter), was added to the TDO plates. Plates were grown at 30°C for 3 d.

Split Ubiquitin Assay

For protein–protein interaction studies between CNGC19 and PEPR1/PEPR2/BAK1, pDONR207 clones were generated by BP Clonase reaction. For split ubiquitin assay, CNGC19 was subcloned into pMETYC vector (Grefen et al., 2009) using LR Clonase to generate the CNGC19:Cub construct, while PEPR1/PEPR2/BAK1 were cloned similarly into pXN22 vector to generate Nub constructs. CNGC19 and other constructs including empty vectors were transformed in mating yeast strains THY.AP4 and THY.AP5, respectively, and plated on appropriate dropout-media–containing plates. For protein–protein interaction studies, THY.AP4 harboring CNGC19:Cub and THY.AP5 with other constructs was allowed for mating in Yeast extract-Peptone-Dextrose medium and then plated on synthetic complete (SC) medium (lacking −Ade, −His, −Trp, and −Leu) and SC+AH containing plates to check the interaction. Empty Nub vector and CNGC19 fused with NubWt served as the negative and positive controls for the experiment.

BiFC Assay

The full-length cDNA fragments (without stop codon) of PEPRs (PEPR1 and PEPR2), BAK1, CaMs (CaM1, CaM2, CaM3, CaM4, CaM6, and CaM7), and CML42 were amplified using the attB adaptor-bearing PCR primers listed in Supplemental Table 1 and cloned into the Gateway entry vector pDONR 207 by BP Clonase reaction (Invitrogen). For BiFC experiments, CNGC19 was cloned into pSITE-nEYFP-N1 (CD3-1650; Martin et al., 2009) using LR Clonase to generate the CNGC19:nEYFP construct, while CaMs and CML42, respectively, were cloned similarly into pSITE-cEYFP-C1 (CD3-1649) to generate cEYFP constructs. For CNGC19 and PEPRs interaction studies, PEPR1, PEPR2, BAK1, and CaM2, respectively, were cloned into pSITE-cEYFP-N1 (CD3-1651) to generate cEYFP constructs. All BIFC constructs and empty vectors were transformed in Agrobacterium strain GV3101. For *N. benthamiana* transient expression, overnight grown cell cultures were harvested and resuspended in the above-mentioned infiltration buffer to optical density (OD_{600}) 0.8. The working suspensions were prepared by mixing appropriate clones containing the BiFC constructs and the gene-silencing inhibitor p19 at 1:1:1 ratio and incubated for 3 h at room temperature. The *A. tumefaciens* suspensions were then coinfiltrated into the abaxial surface of *N. benthamiana* leaves. Infiltrated leaf areas were examined using a SP5 Confocal Microscope (Leica) at 3 d postinoculation. For fluorescence quantification, 6-mm leaf discs were cut out of the infiltrated areas and placed in a black 96-well plate. Fluorescence intensities of leaf discs were measured in a FLUOstar Omega Plate Reader (BMG LABTECH) using a 485- ± 12-nm excitation and a 520-nm emission filter.

Microarray

Total RNA was isolated from 24 h *S. litura* larvae fed on Col-0 wild type and *cngc19-2* leaf tissues using an RNeasy Plant Mini Kit (QIAGEN) from three independent biological replicate pools. RNA samples were checked and quantified by agarose gel, nano drop (Thermo Fisher Scientific), and Agilent 2100 Bioanalyzer (Agilent Technologies). Bioanalyzer quality-test–passed RNA samples (RIN > 7) were used for microarray experiment. GeneChips were scanned using a GeneChip Scanner 3000 7G (Affymetrix) and GeneChip Command Console Software (AGCC v3.2.4; Affymetrix), and six CEL files were generated. All six CEL files were normalized in freely available Expression Console software v.1.3.1 (Affymetrix) using the Robust Multi-array Average algorithm, and probe-set summarization files (CHP files) were generated for genes. The normalized CHP files were processed using the freely available secondary analysis tool, Transcriptome Analysis Console software v.3.1.0.5 (Affymetrix), to generate the .csv files containing differentially expressed genes using the combined criteria of >1.5-fold change with ANOVA *P* value of <0.05. GO enrichment for various differentially expressed transcripts was performed using the BiNGO plug-in (v3.0.3) on the Cytoscape platform (v3.2.1; http://www.cytoscape.org/). Arabidopsis GO information for biological process and molecular function was used for GO enrichment analysis. We considered a *P* value cutoff of ≤0.05 as significant and applied the hypergeometric test to identify enriched GO terms in BiNGO. The software MapMan (v3.5.1; https://mapman.gabipd.org/) was used for functional annotation of differentially expressed transcripts. Heat maps were generated by the software MeV_4_9_0 (https://sourceforge.net/projects/mev-tm4/files/mev-tm4/MeV%204.9.0/).

Statistical Analysis

Statistical differences between different groups were detected by one-way ANOVA and a posthoc Student-Newman-Keuls-(SNK) test or Student's *t* test in the software SigmaStat 2.03 (Systat Software). Different letters indicate significant difference between treatments.

Accession Numbers

The TAIR accession numbers of major genes mentioned in this study are as follows: CNGC19 (At3g17690), CNGC20 (At3g17700), BCAT4 (AT3g19710), PEPR1 (At1g73080), PEPR2 (At1g17750), and CaM2 (AT2g41110).

Supplemental Data

Supplemental Figure 1. Arabidopsis CNGC expression analysis upon simulated herbivory.

Supplemental Figure 2. Verification of *cngc19* T-DNA insertion lines.

Supplemental Figure 3. CNGC20 has no functional role in *S. litura* herbivory.

Supplemental Figure 4. *CNGC19* expression coincides with cAMP production in Arabidopsis.

Supplemental Figure 5. Measuring *w*ound-induced cytosolic Ca^{2+} levels in local leaves of the wild type and *cngc19-2* mutant.

Supplemental Figure 6. CNGC19 is expressed in the *Xenopus* oocyte.

Supplemental Figure 7. Subcellular localization of CNGC19 at the plasma membrane.

Supplemental Figure 8. cAMP levels were unaltered in *pepr1 pepr2* mutants upon simulated herbivory.

Supplemental Figure 9. CNGC19 does not interact with PEPRs and BAK1 in planta.

Supplemental Figure 10. Defense-related phytohormone levels upon herbivory in *cngc19* mutants.

Supplemental Figure 11. Functional categorization of differentially expressed genes in microarray.

Supplemental Figure 12. Analysis of CNGC19-CaMs interaction strength on quadruple dropout medium and BiFC.

Supplemental Figure 13. Expression profile of *CaM*s upon simulated herbivory.

Supplemental Table 1. List of primer pairs used in this study.

Supplemental Table 2. GS content in rosette leaves of *cngc19* mutant lines.

Supplemental Table 3. 2-way ANOVA on GS content of *cngc19* mutant lines upon herbivory.

Supplemental Data Set. List of genes up- and downregulated in the microarray of *cngc19* +*S*. *litura*/wild type + *S*. *litura* with functional annotation by the software MapMan.

Supplemental Movie S1. Mechanical wounding in wild-type plant.

Supplemental Movie S2. Mechanical wounding in *cngc19* mutant plant.

Supplemental Movie S3. Mechanical wounding in wild-type plant.

Supplemental Movie S4. Mechanical wounding in *cngc19* mutant plant.

ACKNOWLEDGMENTS

We thank the National Bureau of Agricultural Insect Resources, Bangalore for *S*. *litura* eggs (National Accession number: NBAII-MP-NOC-02); Pradeep Kumar Maurya (National Institute of Plant Genome Research) for rearing Spodoptera; the National Institute of Plant Genome Research Central Instrumentation and Phytotron Facility, Department of Biotechnology-eLibrary Consortium for providing access to e-resources; Sahil Lall and Central Imaging and Flow Facility (National Centre for Biological Sciences) for *Xenopus* oocyte images; Suneel Katariya (Jawaharlal Nehru University) for help with cAMP quantification; Monika Heyer and Andrea Lehr (Max Planck Institute for Chemical Ecology) for help with phytohormone extraction; Dale Sanders (John Innes Centre, UK) for GCaMP3 lines; Gerald Berkowitz (University of Connecticut, U.S.) for *pepr1 pepr2* mutant; Stefan Binder (University of Ulm, Germany) for *bcat4* mutant line SALK_013627; and Guillermo Hugo Jimenez-Aleman (Max Planck Institute for Chemical Ecology, Jena) for chemically synthesized JA-Ile. This work was supported by the Department of Biotechnology, India through the National Institute of Plant Genome Research Core and BioCare grants (BT/PR18059/BIC/101/994/2016); the Max Planck Gesellschaft-India Partner Group program of the Max Planck Society (Germany) and Department of Science and Technology, India (DST/INT/MPG/P-28/2015); and Department of Biotechnology-Junior Research Fellowship (to R.P.).

AUTHOR CONTRIBUTIONS

J.V. and M.M. designed research; M.M., D.K., and R.P. performed research; K.D., Y.P., and M.K.M. carried out the electrophysiology work; M.R. carried out chemical analyses; M.M., R.P., A.M.,W.B., M.K.M., and J.V. analyzed data; J.V. wrote the article with input from all the authors.

Received January 29, 2019; revised April 18, 2019; accepted May 7, 2019; published May 13, 2019.

REFERENCES

Albert, M. (2013). Peptides as triggers of plant defence. J. Exp. Bot. **64:** 5269–5279.

Alonso, J.M., et al. (2003) Genome-wide insertional mutagenesis of *Arabidopsis thaliana*. Science **301:** 653–657.

Andersen, T.G., Nour-Eldin, H.H., Fuller, V.L., Olsen, C.E., Burow, M., and Halkier, B.A. (2013). Integration of biosynthesis and long-distance transport establish organ-specific glucosinolate profiles in vegetative Arabidopsis. Plant Cell **25:** 3133–3145.

Angelovici, R., Lipka, A.E., Deason, N., Gonzalez-Jorge, S., Lin, H., Cepela, J., Buell, R., Gore, M.A., and Dellapenna, D. (2013). Genome-wide analysis of branched-chain amino acid levels in Arabidopsis seeds. Plant Cell **25:** 4827–4843.

Balagué, C., Lin, B., Alcon, C., Flottes, G., Malmström, S., Köhler, C., Neuhaus, G., Pelletier, G., Gaymard, F., and Roby, D. (2003). HLM1, an essential signaling component in the hypersensitive response, is a member of the cyclic nucleotide-gated channel ion channel family. Plant Cell **15:** 365–379.

Bartels, S., Lori, M., Mbengue, M., van Verk, M., Klauser, D., Hander, T., Böni, R., Robatzek, S., and Boller, T. (2013). The family of Peps and their precursors in Arabidopsis: Differential expression and localization but similar induction of pattern-triggered immune responses. J. Exp. Bot. **64:** 5309–5321.

Bergomaz, R., and Boppré, M. (1986). A simple instant diet for rearing *Arctiidae* and other moths. J. Lepidopterists Soc. **40:** 131–137.

Boller, T., and Felix, G. (2009). A renaissance of elicitors: Perception of microbe-associated molecular patterns and danger signals by pattern-recognition receptors. Annu. Rev. Plant Biol. **60:** 379–406.

Brown, P.D., Tokuhisa, J.G., Reichelt, M., and Gershenzon, J. (2003). Variation of glucosinolate accumulation among different organs and developmental stages of *Arabidopsis thaliana*. Phytochemistry **62:** 471–481.

Burow, M., Müller, R., Gershenzon, J., and Wittstock, U. (2006). Altered glucosinolate hydrolysis in genetically engineered *Arabidopsis thaliana* and its influence on the larval development of *Spodoptera littoralis*. J. Chem. Ecol. **32:** 2333–2349.

Burow, M., Atwell, S., Francisco, M., Kerwin, R.E., Halkier, B.A., and Kliebenstein, D.J. (2015). The glucosinolate biosynthetic gene *AOP2* mediates feed-back regulation of jasmonic acid signaling in Arabidopsis. Mol. Plant **8:** 1201–1212.

Cheng, T., et al. (2017) Genomic adaptation to polyphagy and insecticides in a major East Asian noctuid pest. Nat. Ecol. Evol. **1:** 1747–1756.

Chiasson, D.M., Haage, K., Sollweck, K., Brachmann, A., Dietrich, P., and Parniske, M. (2017). A quantitative hypermorphic *CNGC* allele confers ectopic calcium flux and impairs cellular development. eLife **6:** e25012.

Clough, S.J., and Bent, A.F. (1998). Floral dip: a simplified method for *Agrobacterium*-mediated transformation of *Arabidopsis thaliana*. Plant J. **16:** 735–743.

Clough, S.J., Fengler, K.A., Yu, I.C., Lippok, B., Smith, R.K., Jr., and Bent, A.F. (2000). The Arabidopsis *dnd1* "defense, no death" gene encodes a mutated cyclic nucleotide-gated ion channel. Proc. Natl. Acad. Sci. USA **97:** 9323–9328.

Crocoll, C., Mirza, N., Reichelt, M., Gershenzon, J., and Halkier, B.A. (2016). Optimization of engineered production of the glucoraphanin precursor dihomomethionine in *Nicotiana benthamiana*. Front. Bioeng. Biotechnol. **4:** 14.

DeFalco, T.A., Marshall, C.B., Munro, K., Kang, H.G., Moeder, W., Ikura, M., Snedden, W.A., and Yoshioka, K. (2016). Multiple calmodulin-binding sites positively and negatively regulate Arabidopsis CYCLIC NUCLEOTIDE-GATED CHANNEL12. Plant Cell **28:** 1738–1751.

Demidchik, V., Shabala, S., Isayenkov, S., Cuin, T.A., and Pottosin, I. (2018). Calcium transport across plant membranes: Mechanisms and functions. New Phytol. **220:** 49–69.

Dodd, A.N., Kudla, J., and Sanders, D. (2010). The language of calcium signaling. Annu. Rev. Plant Biol. **61:** 593–620.

Earley, K.W., Haag, J.R., Pontes, O., Opper, K., Juehne, T., Song, K., and Pikaard, C.S. (2006). Gateway-compatible vectors for plant functional genomics and proteomics. Plant J. **45:** 616–629.

Fand, B.B., Sul, N.T., Bal, S.K., and Minhas, P.S. (2015). Temperature impacts the development and survival of common cutworm (*Spodoptera litura*): Simulation and visualization of potential

population growth in India under warmer temperatures through life cycle modelling and spatial mapping. PLoS One **10:** e0124682.

Fischer, C., Kugler, A., Hoth, S., and Dietrich, P. (2013). An IQ domain mediates the interaction with calmodulin in a plant cyclic nucleotide-gated channel. Plant Cell Physiol. **54:** 573–584.

Fischer, C., DeFalco, T.A., Karia, P., Snedden, W.A., Moeder, W., Yoshioka, K., and Dietrich, P. (2017). Calmodulin as a Ca^{2+}-sensing subunit of Arabidopsis cyclic nucleotide-gated channel complexes. Plant Cell Physiol. **58:** 1208–1221.

Gao, Q.F., Gu, L.L., Wang, H.Q., Fei, C.F., Fang, X., Hussain, J., Sun, S.J., Dong, J.Y., Liu, H., and Wang, Y.F. (2016). Cyclic nucleotide-gated channel 18 is an essential Ca^{2+} channel in pollen tube tips for pollen tube guidance to ovules in *Arabidopsis*. Proc. Natl. Acad. Sci. USA **113:** 3096–3101.

Genger, R.K., Jurkowski, G.I., McDowell, J.M., Lu, H., Jung, H.W., Greenberg, J.T., and Bent, A.F. (2008). Signaling pathways that regulate the enhanced disease resistance of Arabidopsis "defense, no death" mutants. Mol. Plant Microbe Interact. **21:** 1285–1296.

Gfeller, A., Baerenfaller, K., Loscos, J., Chételat, A., Baginsky, S., and Farmer, E.E. (2011). Jasmonate controls polypeptide patterning in undamaged tissue in wounded Arabidopsis leaves. Plant Physiol. **156:** 1797–1807.

Grefen, C., Obrdlik, P., and Harter, K. (2009). The determination of protein–protein interactions by the mating-based split-ubiquitin system (mbSUS). Methods Mol. Biol. **479:** 217–233.

Huffaker, A., and Ryan, C.A. (2007). Endogenous peptide defense signals in Arabidopsis differentially amplify signaling for the innate immune response. Proc. Natl. Acad. Sci. USA **104:** 10732–10736.

Jurkowski, G.I., Smith, R.K., Jr., Yu, I.C., Ham, J.H., Sharma, S.B., Klessig, D.F., Fengler, K.A., and Bent, A.F. (2004). Arabidopsis *DND2*, a second cyclic nucleotide-gated ion channel gene for which mutation causes the "*defense*, *no death*" phenotype. Mol. Plant Microbe Interact. **17:** 511–520.

Kaplan, B., Sherman, T., and Fromm, H. (2007). Cyclic nucleotide-gated channels in plants. FEBS Lett. **581:** 2237–2246.

Kiep, V., Vadassery, J., Lattke, J., Maaß, J.P., Boland, W., Peiter, E., and Mithöfer, A. (2015). Systemic cytosolic Ca^{2+} elevation is activated upon wounding and herbivory in Arabidopsis. New Phytol. **207:** 996–1004.

Klauser, D., Desurmont, G.A., Glauser, G., Vallat, A., Flury, P., Boller, T., Turlings, T.C., and Bartels, S. (2015). The Arabidopsis Pep-PEPR system is induced by herbivore feeding and contributes to JA-mediated plant defence against herbivory. J. Exp. Bot. **66:** 5327–5336.

Kliebenstein, D.J., Kroymann, J., Brown, P., Figuth, A., Pedersen, D., Gershenzon, J., and Mitchell-Olds, T. (2001). Genetic control of natural variation in Arabidopsis glucosinolate accumulation. Plant Physiol. **126:** 811–825.

Knight, H., Trewavas, A.J., and Knight, M.R. (1997). Calcium signalling in *Arabidopsis thaliana* responding to drought and salinity. Plant J. **12:** 1067–1078.

Krol, E., Mentzel, T., Chinchilla, D., Boller, T., Felix, G., Kemmerling, B., Postel, S., Arents, M., Jeworutzki, E., Al-Rasheid, K.A., Becker, D., and Hedrich, R. (2010). Perception of the Arabidopsis danger signal peptide 1 involves the pattern recognition receptor *At*PEPR1 and its close homologue *At*PEPR2. J. Biol. Chem. **285:** 13471–13479.

Kugler, A., Köhler, B., Palme, K., Wolff, P., and Dietrich, P. (2009). Salt-dependent regulation of a CNG channel subfamily in Arabidopsis. BMC Plant Biol. **9:** 140.

Lächler, K., Imhof, J., Reichelt, M., Gershenzon, J., and Binder, S. (2015). The cytosolic branched-chain aminotransferases of *Arabidopsis thaliana* influence methionine supply, salvage and glucosinolate metabolism. Plant Mol. Biol. **88:** 119–131.

Laluk, K., Prasad, K.V., Savchenko, T., Celesnik, H., Dehesh, K., Levy, M., Mitchell-Olds, T., and Reddy, A.S. (2012). The calmodulin-binding transcription factor SIGNAL RESPONSIVE1 is a novel regulator of glucosinolate metabolism and herbivory tolerance in Arabidopsis. Plant Cell Physiol. **53:** 2008–2015.

Lan, Z., Krosse, S., Achard, P., van Dam, N.M., and Bede, J.C. (2014). DELLA proteins modulate Arabidopsis defences induced in response to caterpillar herbivory. J. Exp. Bot. **65:** 571–583.

Landoni, M., De Francesco, A., Galbiati, M., and Tonelli, C. (2010). A loss-of-function mutation in Calmodulin2 gene affects pollen germination in *Arabidopsis thaliana*. Plant Mol. Biol. **74:** 235–247.

Lee, D., Polisensky, D.H., and Braam, J. (2005). Genome-wide identification of touch- and darkness-regulated Arabidopsis genes: A focus on calmodulin-like and XTH genes. New Phytol. **165:** 429–444.

Levy, M., Wang, Q., Kaspi, R., Parrella, M.P., and Abel, S. (2005). Arabidopsis IQD1, a novel calmodulin-binding nuclear protein, stimulates glucosinolate accumulation and plant defense. Plant J. **43:** 79–96.

Liu, K., and Luan, S. (2001). Internal aluminum block of plant inward K^+ channels. Plant Cell **13:** 1453–1465.

Lu, M., Zhang, Y., Tang, S., Pan, J., Yu, Y., Han, J., Li, Y., Du, X., Nan, Z., and Sun, Q. (2016). *AtCNGC2* is involved in jasmonic acid-induced calcium mobilization. J. Exp. Bot. **67:** 809–819.

Ma, Y., Walker, R.K., Zhao, Y., and Berkowitz, G.A. (2012). Linking ligand perception by PEPR pattern recognition receptors to cytosolic Ca^{2+} elevation and downstream immune signaling in plants. Proc. Natl. Acad. Sci. USA **109:** 19852–19857.

Maffei, M., Bossi, S., Spiteller, D., Mithöfer, A., and Boland, W. (2004). Effects of feeding *Spodoptera littoralis* on lima bean leaves. I. Membrane potentials, intracellular calcium variations, oral secretions, and regurgitate components. Plant Physiol. **134:** 1752–1762.

Martin, K., Kopperud, K., Chakrabarty, R., Banerjee, R., Brooks, R., and Goodin, M.M. (2009). Transient expression in *Nicotiana benthamiana* fluorescent marker lines provides enhanced definition of protein localization, movement and interactions *in planta*. Plant J. **59:** 150–162.

Mäser, P., et al. (2001) Phylogenetic relationships within cation transporter families of Arabidopsis. Plant Physiol. **126:** 1646–1667.

McCormack, E., and Braam, J. (2003). Calmodulins and related potential calcium sensors of Arabidopsis. New Phytol. **159:** 585–598.

McCormack, E., Tsai, Y.C., and Braam, J. (2005). Handling calcium signaling: Arabidopsis CaMs and CMLs. Trends Plant Sci. **10:** 383–389.

Meena, M.K., and Vadassery, J. (2015). Channels hold the key: Cyclic nucleotide gated channels (CNGC) in plant biotic stress signaling. Endocytobiosis Cell Res. **26:** 25–30.

Mithöfer, A., and Boland, W. (2012). Plant defense against herbivores: Chemical aspects. Annu. Rev. Plant Biol. **63:** 431–450.

Mousavi, S.A., Chauvin, A., Pascaud, F., Kellenberger, S., and Farmer, E.E. (2013). GLUTAMATE RECEPTOR-LIKE genes mediate leaf-to-leaf wound signalling. Nature **500:** 422–426.

Müller, R., de Vos, M., Sun, J.Y., Sønderby, I.E., Halkier, B.A., Wittstock, U., and Jander, G. (2010). Differential effects of indole and aliphatic glucosinolates on lepidopteran herbivores. J. Chem. Ecol. **36:** 905–913.

Nelson, B.K., Cai, X., and Nebenführ, A. (2007). A multicolored set of *in vivo* organelle markers for co-localization studies in Arabidopsis and other plants. Plant J. **51:** 1126–1136.

Nguyen, C.T., Martinoia, E., and Farmer, E.E. (2017). Emerging jasmonate transporters. Mol. Plant **10:** 659–661.

Nguyen, C.T., Kurenda, A., Stolz, S., Chételat, A., and Farmer, E.E. (2018). Identification of cell populations necessary for leaf-to-leaf

electrical signaling in a wounded plant. Proc. Natl. Acad. Sci. USA **115:** 10178–10183.

Qi, Z., Verma, R., Gehring, C., Yamaguchi, Y., Zhao, Y., Ryan, C.A., and Berkowitz, G.A. (2010). Ca^{2+} signaling by plant *Arabidopsis thaliana* Pep peptides depends on AtPepR1, a receptor with guanylyl cyclase activity, and cGMP-activated Ca^{2+} channels. Proc. Natl. Acad. Sci. USA **107:** 21193–21198.

Rao, X., Huang, X., Zhou, Z., and Lin, X. (2013). An improvement of the $2(-\Delta\Delta CT)$ method for quantitative real-time polymerase chain reaction data analysis. Biostat. Bioinforma. Biomath. **3:** 71–85.

Rentel, M.C., and Knight, M.R. (2004). Oxidative stress-induced calcium signaling in Arabidopsis. Plant Physiol. **135:** 1471–1479.

Scholz, S.S., Vadassery, J., Heyer, M., Reichelt, M., Bender, K.W., Snedden, W.A., Boland, W., and Mithöfer, A. (2014). Mutation of the Arabidopsis calmodulin-like protein CML37 deregulates the jasmonate pathway and enhances susceptibility to herbivory. Mol. Plant **7:** 1712–1726.

Scholz, S.S., Malabarba, J., Reichelt, M., Heyer, M., Ludewig, F., and Mithöfer, A. (2017). Evidence for GABA-induced systemic GABA accumulation in Arabidopsis upon wounding. Front. Plant Sci. **8:** 388.

Schuster, J., Knill, T., Reichelt, M., Gershenzon, J., and Binder, S. (2006). Branched-chain aminotransferase4 is part of the chain elongation pathway in the biosynthesis of methionine-derived glucosinolates in Arabidopsis. Plant Cell **18:** 2664–2679.

Seybold, H., Trempel, F., Ranf, S., Scheel, D., Romeis, T., and Lee, J. (2014). Ca^{2+} signalling in plant immune response: From pattern recognition receptors to Ca^{2+} decoding mechanisms. New Phytol. **204:** 782–790.

Sheard, L.B., et al. (2010) Jasmonate perception by inositol-phosphate-potentiated COI1-JAZ co-receptor. Nature **468:** 400–405.

Shroff, R., Vergara, F., Muck, A., Svatos, A., and Gershenzon, J. (2008). Nonuniform distribution of glucosinolates in *Arabidopsis thaliana* leaves has important consequences for plant defense. Proc. Natl. Acad. Sci. USA **105:** 6196–6201.

Swarbreck, S.M., Colaço, R., and Davies, J.M. (2013). Plant calcium-permeable channels. Plant Physiol. **163:** 514–522.

Tan, Q., Zhang, L., Grant, J., Cooper, P., and Tegeder, M. (2010). Increased phloem transport of S-methylmethionine positively affects sulfur and nitrogen metabolism and seed development in pea plants. Plant Physiol. **154:** 1886–1896.

Textor, S., and Gershenzon, J. (2009). Herbivore induction of the glucosinolate-myrosinase defense system: Major trends, biochemical bases and ecological significance. Phytochem. Rev. **8:** 149–170.

Toyota, M., Spencer, D., Sawai-Toyota, S., Jiaqi, W., Zhang, T., Koo, A.J., Howe, G.A., and Gilroy, S. (2018). Glutamate triggers long-distance, calcium-based plant defense signaling. Science **361:** 1112–1115.

Urquhart, W., Gunawardena, A.H.L.A.N., Moeder, W., Ali, R., Berkowitz, G.A., and Yoshioka, K. (2007). The chimeric cyclic nucleotide-gated ion channel ATCNGC11/12 constitutively induces programmed cell death in a Ca^{2+} dependent manner. Plant Mol. Biol. **65:** 747–761.

Vadassery, J., Reichelt, M., Hause, B., Gershenzon, J., Boland, W., and Mithöfer, A. (2012). CML42-mediated calcium signaling coordinates responses to Spodoptera herbivory and abiotic stresses in Arabidopsis. Plant Physiol. **159:** 1159–1175.

Vadassery, J., Reichelt, M., Jimenez-Aleman, G.H., Boland, W., and Mithöfer, A. (2014). Neomycin inhibition of (+)-7-iso-jasmonoyl-L-isoleucine accumulation and signaling. J. Chem. Ecol. **40:** 676–686.

Van Poecke, R.M.P. (2007). Arabidopsis–insect interactions. Arabidopsis Book **5:** e0107.

Vincent, T.R., Avramova, M., Canham, J., Higgins, P., Bilkey, N., Mugford, S.T., Pitino, M., Toyota, M., Gilroy, S., Miller, A.J., Hogenhout, S.A., and Sanders, D. (2017). Interplay of plasma membrane and vacuolar ion channels, together with BAK1, elicits rapid cytosolic calcium elevations in Arabidopsis during aphid feeding. Plant Cell **29:** 1460–1479.

Walter, A., Mazars, C., Maitrejean, M., Hopke, J., Ranjeva, R., Boland, W., and Mithöfer, A. (2007). Structural requirements of jasmonates and synthetic analogues as inducers of Ca^{2+} signals in the nucleus and the cytosol of plant cells. Angew. Chem. Int. Ed. Engl. **46:** 4783–4785.

Wasternack, C., and Hause, B. (2013). Jasmonates: Biosynthesis, perception, signal transduction and action in plant stress response, growth and development. An update to the 2007 review in *Annals of Botany*. Ann. Bot. **111:** 1021–1058.

Wudick, M.M., Portes, M.T., Michard, E., Rosas-Santiago, P., Lizzio, M.A., Nunes, C.O., Campos, C., Santa Cruz Damineli, D., Carvalho, J.C., Lima, P.T., Pantoja, O., and Feijó, J.A. (2018). CORNICHON sorting and regulation of GLR channels underlie pollen tube Ca^{2+} homeostasis. Science **360:** 533–536.

Xie, D.X., Feys, B.F., James, S., Nieto-Rostro, M., and Turner, J.G. (1998). COI1: An Arabidopsis gene required for jasmonate-regulated defense and fertility. Science **280:** 1091–1094.

Yamaguchi, Y., Pearce, G., and Ryan, C.A. (2006). The cell surface leucine-rich repeat receptor for *At*Pep1, an endogenous peptide elicitor in Arabidopsis, is functional in transgenic tobacco cells. Proc. Natl. Acad. Sci. USA **103:** 10104–10109.

Yamaguchi, Y., Huffaker, A., Bryan, A.C., Tax, F.E., and Ryan, C.A. (2010). PEPR2 is a second receptor for the Pep1 and Pep2 peptides and contributes to defense responses in *Arabidopsis*. Plant Cell **22:** 508–522.

Yan, C., Fan, M., Yang, M., Zhao, J., Zhang, W., Su, Y., Xiao, L., Deng, H., and Xie, D. (2018). Injury activates Ca^{2+}/calmodulin-dependent phosphorylation of JAV1-JAZ8-WRKY51 complex for jasmonate biosynthesis. Mol. Cell **70:** 136–149.e7.

Yoshioka, K., Kachroo, P., Tsui, F., Sharma, S.B., Shah, J., and Klessig, D.F. (2001). Environmentally sensitive, SA-dependent defense responses in the cpr22 mutant of Arabidopsis. Plant J. **26:** 447–459.

Yuen, C.C.Y., and Christopher, D.A. (2013). The group IV-A cyclic nucleotide-gated channels, CNGC19 and CNGC20, localize to the vacuole membrane in *Arabidopsis thaliana*. AoB Plants **5:** 1–14.

Zebelo, S.A., and Maffei, M.E. (2015). Role of early signalling events in plant-insect interactions. J. Exp. Bot. **66:** 435–448.

Zhang, C., Beckmann, L., Kudla, J., and Batistič, O. (2017a). N-terminal S-acylation facilitates tonoplast targeting of the calcium sensor CBL6. FEBS Lett. **591:** 3745–3756.

Zhang, S., Pan, Y., Tian, W., Dong, M., Zhu, H., Luan, S., and Li, L. (2017b). Arabidopsis CNGC14 mediates calcium influx required for tip growth in root hairs. Mol. Plant **10:** 1004–1006.

Zhang, W., Zhou, R.G., Gao, Y.J., Zheng, S.Z., Xu, P., Zhang, S.Q., and Sun, D.Y. (2009). Molecular and genetic evidence for the key role of AtCaM3 in heat-shock signal transduction in Arabidopsis. Plant Physiol. **149:** 1773–1784.

Zhou, L., Lan, W., Jiang, Y., Fang, W., and Luan, S. (2014). A calcium-dependent protein kinase interacts with and activates a calcium channel to regulate pollen tube growth. Mol. Plant **7:** 369–376.

Zimmermann, M.R., Maischak, H., Mithöfer, A., Boland, W., and Felle, H.H. (2009). System potentials, a novel electrical long-distance apoplastic signal in plants, induced by wounding. Plant Physiol. **149:** 1593–1600.

Zimmermann, M.R., Mithöfer, A., Will, T., Felle, H.H., and Furch, A.C.U. (2016). Herbivore-triggered electrophysiological reactions: Candidates for systemic signals in higher plants and the challenge of their identification. Plant Physiol. **170:** 2407–2419.

The Ca^{2+} Channel CNGC19 Regulates Arabidopsis Defense Against Spodoptera Herbivory

Mukesh Kumar Meena, Ramgopal Prajapati, Deepthi Krishna, Keerthi Divakaran, Yogesh Pandey, Michael Reichelt, M.K. Mathew, Wilhelm Boland, Axel Mithöfer and Jyothilakshmi Vadassery

Plant Cell 2019;31;1539-1562; originally published online May 10, 2019;
DOI 10.1105/tpc.19.00057